UNCLASSIFIED

ORNL 1068
Physics and Mathematics
9u

MARTIN MARIETTA ENERGY SYSTEMS LIBRARIES
3 4456 0352784 1

THE TOTAL NEUTRON CROSS SECTION OF HOLMIUM AS A FUNCTION OF ENERGY

OAK RIDGE NATIONAL LABORATORY
CENTRAL RESEARCH LIBRARY
CIRCULATION SECTION
4500N ROOM 175
LIBRARY LOAN COPY
DO NOT TRANSFER TO ANOTHER PERSON
If you wish someone else to see this report, send in name with report and the library will arrange a loan.
ORNL-RL 1475

OAK RIDGE NATIONAL LABORATORY
OPERATED BY
CARBIDE AND CARBON CHEMICALS COMPANY
A DIVISION OF UNION CARBIDE AND CARBON CORPORATION
UCC
POST OFFICE BOX P
OAK RIDGE, TENNESSEE

UNCLASSIFIED

UNCLASSIFIED

ORNL-1068

This document consists of 77 pages. Copy 2 of 260.
Series A.

Contract No. W-7405, eng. 26

PHYSICS DIVISION

THE TOTAL NEUTRON CROSS SECTION OF HOLMIUM AS A FUNCTION OF ENERGY

T. E. Stephenson

DATE ISSUED

OAK RIDGE NATIONAL LABORATORY
Operated by
CARBIDE AND CARBON CHEMICALS DIVISION
Union Carbide and Carbon Corporation
Post Office Box P
Oak Ridge, Tennessee

* A thesis submitted to the Committee on Graduate Study of the University of Tennessee in partial fulfillment of the requirements for the degree of Master of Science, August 1950.

UNCLASSIFIED

MARTIN MARIETTA ENERGY SYSTEMS LIBRARIES
3 4456 0352784 1

INTERNAL DISTRIBUTION

1. G. T. Felbeck (C&CCC)
2-3. Chemistry Library
4. Physics Library
5. Biology Library
6. Health Physics Library
7. Metallurgy Library
8-9. Training School Library
10-13. Central Files
14. C. E. Center
15. C. E. Larson
16. W. B. Humes (K-25)
17. W. D. Lavers (Y-12)
18. A. M. Weinberg
19. E. H. Taylor
20. E. D. Shipley
21. A. H. Snell
22. F. C. VonderLage
23. R. C. Briant
24. J. A. Swartout
25. S. C. Lind
26. F. L. Steahly
27. A. Hollaender
28. M. T. Kelley
29. G. H. Clewett
30. K. Z. Morgan
31. J. S. Felton
32. A. S. Householder
33. C. S. Harrill
34. C. E. Winters
35. D. S. Billington
36. D. W. Cardwell
37. E. M. King
38. E. O. Wollan
39. C. B. Ellis
40. L. D. Roberts
41. R. N. Lyon
42. W. C. Koehler
43. W. K. Ergen
44. E. P. Blizard
45. M. E. Rose
46-95. T. E. Stephenson
96. M. J. Skinner
97-98. Central Files (O.P.)

EXTERNAL DISTRIBUTION

99-110. Argonne National Laboratory
111. Armed Forces Special Weapons Project
112-117. Atomic Energy Commission, Washington
118. Battelle Memorial Institute
119. Brush Beryllium Company
120-123. Brookhaven National Laboratory
124. Bureau of Medicine and Surgery
125. Bureau of Ships
126-129. Carbide and Carbon Chemicals Company (K-25 Plant)
130-133. Carbide and Carbon Chemicals Company (Y-12 Plant)
134. Columbia University (J. R. Dunning)
135. Columbia University (G. Failla)
136-140. E. I. duPont deNemours and Company
141-144. General Electric, Richland
145-148. Idaho Operations Office
149-150. Iowa State College
151. Kansas City Operations Branch
152. Kellex Corporation
153-154. Kirtland Air Force Base
155-158. Knolls Atomic Power Laboratory
159-161. Los Alamos Scientific Laboratory
162. Mallinckrodt Chemical Works
163. Massachusetts Institute of Technology (A. Gaudin)
164. Massachusetts Institute of Technology (A. R. Kaufmann)
165-167. Mound Laboratory
168. National Advisory Committee for Aeronautics
169. National Bureau of Standards (R. D. Huntoon)
170. Naval Medical Research Institute
171-172. Naval Radiological Defense Laboratory
173. New Brunswick Laboratory
174-176. New York Operations Office
177. North American Aviation, Inc.
178. Patent Branch, Washington

179. RAND Corporation
180. Sandia Corporation
181. Sante Fe Operations Office
182. Savannah River Operations Office (Wilmington)
183-197. Technical Information Service, Oak Ridge
198-199. U. S. Geological Survey (T. B. Nolan)
200-201. U. S. Public Health Service
202. University of California at Los Angeles
203-207. University of California Radiation Laboratory
208-209. University of Rochester
210. University of Washington
211. Western Reserve University
212-215. Westinghouse Electric Corporation
216. Yale University
217-220. Atomic Energy Project, Chalk River
221. Chief of Naval Research
222. H. K. Ferguson Company
223. Harshaw Chemical Company
224. Isotopes Division (Mr. McCormick)
225-226. Library of Congress, Acquisition Department (J. W. Cormn)
227. National Bureau of Standards
228. National Research Council, Ottawa
229. Naval Research Laboratory
230-231. Nevis Cyclotron Laboratories
232-233. Oak Ridge Institute of Nuclear Studies
234-243. United Kingdom Scientific Mission (M. Greenhill)
244. USAF, Eglin Air Force Base (Technical Library)
245. USAF, Wright-Patterson Air Force Base (Rodney Nudenberg)
246-250. USAF, Wright-Patterson Air Force Base (CADO)
251. U. S. Army, Army Field Forces (Captain James Kerr)
252. U. S. Army, Atomic Energy Branch (Lt. Col. A. W. Betts)
253. U. S. Army, Director of Operations Research (Dr. Ellis Johnson)
254. U. S. Army, Office, Chief of Ordnance (Col. A. R. Del Campo)
255-256. U. S. Army, Office of the Chief Signal Officer (Curtis T. Clayton through Major George C. Hunt)
257-259. U. S. Army, Technical Command (Col. J. H. Rothschild Attn: Technical Library)
260. UT-AEC Agricultural Research Program (Charles S. Hobbs)

TABLE OF CONTENTS

CHAPTER		PAGE
I.	INTRODUCTION TO THE PROBLEM	8
II.	APPARATUS AND PROCEDURE	12
III.	RESOLUTION.	42
IV.	STATISTICAL ACCURACY.	62
V.	PURITY OF SAMPLE.	66
VI.	RESULTS	67
BIBLIOGRAPHY		77

LIST OF TABLES

TABLE		PAGE
I.	Variation in Glancing Angle for $\theta = 12^{\circ}\ 4'$	57
II.	The Calculated Resolving Power of the Crystal Spectrometer Across the Energy Spectrum.	60
III.	Results of Transmission Measurements on Holmium	68

LIST OF FIGURES

FIGURE		PAGE
1.	The Bent Crystal Spectrometer	13
2.	Neutron Spectrometer Diagram	14
3.	Cadmium Cross Section vs. Energy Measured by Two Tube Method	17
4.	Sample Shifter Showing Wafer in Place	21
5.	Sample Positioning Mechanism	22
6.	Sample Tube Holder	24
7.	Sample Tube	26
8.	Rocking Curves (6 mm Slit)	28
9.	Ratio $\frac{\text{Counts/Sec E}}{\text{Counts/Sec W}}$	29
10.	Absolute Counting Rate vs. Energy for Two mm Capilary and Six mm Slit Width	30
11.	Background vs. Energy 6 mm Slit Width	31
12.	Beam Count/Background	32
13.	Counting Rate vs. Crystal Curvature (5 mm Slit Width)	35
14.	Counting Rate vs. Slit Width	36
15.	Absorption of Reflected Beam in BF_3	38
16.	Schematic Circuit Diagram	40
17.	The Point Source	43
18.	The Finite Source--Case I	46
19.	The Finite Source--Case II	48

FIGURE PAGE

20. The Finite Source--Case III. 49

21. The Finite Slit--Case IV 50

22a. The Point Source and the Crystal 52

22b. The 1.5 Millimeter Source--Case I. 52

22c. The 1.5 Millimeter Source--Case II 52

23a. The 1.5 Millimeter Source--Case III. 55

23b. The 1.5 Millimeter Source--Case IV 55

24. The Total Cross Section of Holmium 69

25. The Total Cross Section of Holmium 70

CHAPTER I

INTRODUCTION TO THE PROBLEM

The objective of this experiment is to measure the total neutron cross section of the rare earth, holmium, as a function of neutron energy. Neutron cross sections are of interest for several reasons. For example, when a substance is considered for a nuclear reactor structural material, its neutron cross section is of primary importance. Or if it is being considered for use as a target material for making a desired radioactive isotope, a knowledge of the cross section is useful. The value of the cross section may furnish information about nuclear structure. Measurement of neutron energy associated with resonance gives information about the energy level system of the compound nucleus for excitation energies in the neighborhood of six to eight M.e.v.

The thermal neutron capture cross section of holmium has been measured by W. Bothe,[1] who reports 49 barns, by Seren, Friedlander, and Turkel,[2] who report 59.6 barns, and by H. Pomerance,[3] who reports 64 barns. The first two values were obtained by the activation technique,[4]

---

[1]W. Bothe, Z. Naturforch 1, 179, 1946.

[2]Leo Seren, Herbert N. Friedlander, and Solomon H. Turkel, "Thermal Neutron Activation Cross Sections," The Physical Review, 72:888-901, 1947.

[3]H. Pomerance, To be published.

[4]Seren, Friedlander, and Turkel, loc. cit.

while the latter result was obtained with the pile oscillator.[5] It is believed that the total neutron cross section of holmium as a function of neutron energy has not previously been measured.

The cross section measurements as a function of energy were by the transmission method. This technique requires a collimated and monoenergetic neutron beam. One places a detector in the beam and counts the neutrons with and without the sample in the beam. Background counts are taken for both of these conditions. Then the transmission of the sample is determined as follows:

$$T = \frac{I - \beta}{I_o - \beta_o}$$

where T is the Transmission, $I - \beta$ is the counting rate with the sample in the beam, minus the background for this condition. $I_o - \beta_o$ is the counting rate with no sample in the beam, minus the background for this condition.

The value of the cross section, σ, is calculated from the measured value of the transmission. The relation between the cross section and the transmission may be derived as follows. Consider an infinitesimal thickness, dt, of the absorbing layer of thickness t. Let I be the intensity of the neutron beam incident on the infinitesimal thickness dt. If we assume that a single collision removes the neutron from the beam, the fraction of I which is absorbed in dt is $\frac{dI}{I}$ and

---

[5]J. I. Hoover, W. H. Jordan, C. D. Moak, L. Pardue, H. Pomerance, J. D. Strong, and E. O. Wollan, "Measurement of Neutron Absorption Cross Sections, with a Pile Oscillator," The Physical Review, 74:886-870, 1948.

this is proportional to dt:

$$\frac{dI}{I} = -\alpha\, dt$$

The negative sign is used because the intensity decreases as the beam passes through the absorber. The constant of proportionality, α, is usually called the absorption coefficient in X-ray and gamma ray work. In keeping with the assumption that a single collision removes a neutron from the beam, it would be reasonable to say that α would depend on a property of the atom under consideration, i.e., upon the effective area which the atom presents to the approaching neutron and upon the number of atoms per unit volume.

Let us denote this effective area as σ and the number of atoms per cubic centimeter as n. Then $\alpha = n\sigma$ and the differential equation may be written as follows:

$$\frac{dI}{I} = -n\,\sigma\, dt$$

If we denote the beam intensity which is incident upon the surface of the absorber as I_o, and integrate with respect to the thickness of the absorber, we have:

$$\int_{I_o}^{I} \frac{dI}{I} = -n\,\sigma \int_{o}^{t} dt$$

$$\ln \frac{I}{I_o} = -n\,\sigma\, t$$

$$\frac{I}{I_o} = e^{-nt\sigma}$$

Thus the transmission is

$$T = e^{-nt\sigma}$$

This is the quantity which is measured. The cross section may be calculated from the above expression as follows:

$$\sigma = \frac{-\ln T}{n\ t}$$

The cross section is usually expressed in barns. (One barn = 10^{-24} cm^2.)

CHAPTER II

APPARATUS AND PROCEDURE

In order to obtain beams of nearly monochromatic neutron wave length or energy, a neutron crystal spectrometer was used. This instrument is an old X-ray spectrometer which was originally set up for use with neutrons by L. B. Borst and associates.[1] The instrument was thoroughly overhauled and revamped for use in a program of measuring the total cross sections of small samples of certain rare stable and radioactive isotopes.[2] The results of some of the new features, whose description is given below along with a general description of the apparatus, were to increase the incident neutron intensity and to decrease the background count by large factors, thus permitting the use of smaller samples with much better counting statistics. A photograph of the instrument is given in Figure 1. Figure 2 is a schematic diagram showing the spectrometer in place and its relation to the neutron beam collimator and the sample. The crystal is mounted so that its axis of rotation coincides with the axis of the circular scales and is about fourteen inches from the face of the pile. The counter tube is mounted on an arm so that its distance from the crystal is about five feet. The angular position of the crystal and of the counter can be read to one minute of arc.

---

[1] L. B. Borst, A. J. Ulrich, C. L. Osborne, and B. Hasbrouck, The Physical Review, 70:108, 1946.

[2] S. Bernstein, J. B. Dial, C. P. Stanford, and T. E. Stephenson, "Total Cross Sections of Small Samples of Hf, Er, Ni^{58}, and Ni^{60} from Neutron Crystal Spectrometer Measurements," The Physical Review, 75:1302, 1949.

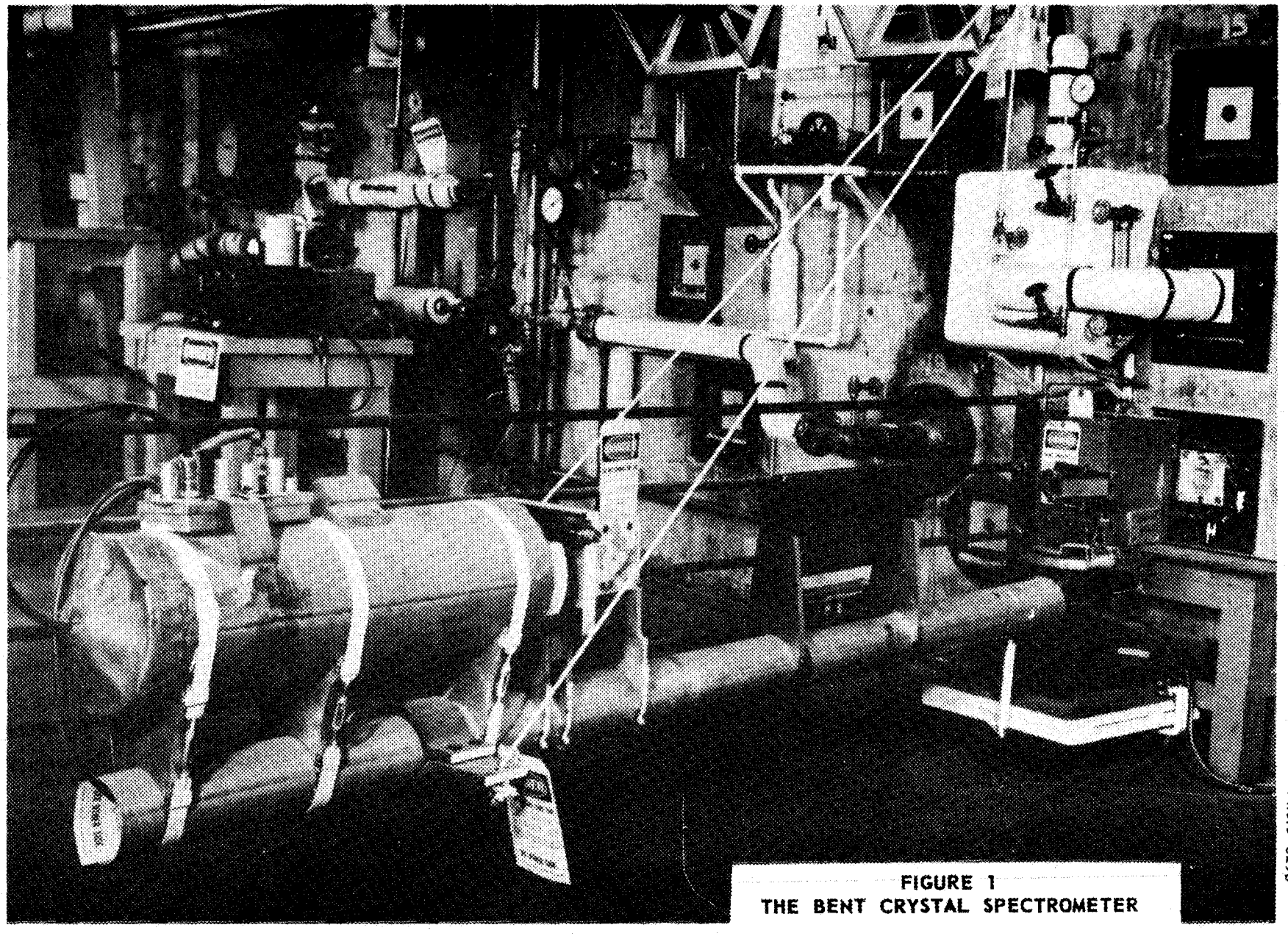

FIGURE 1
THE BENT CRYSTAL SPECTROMETER

UNCLASSIFIED
Photo 3296

UNCLASSIFIED
Dwg. 6246

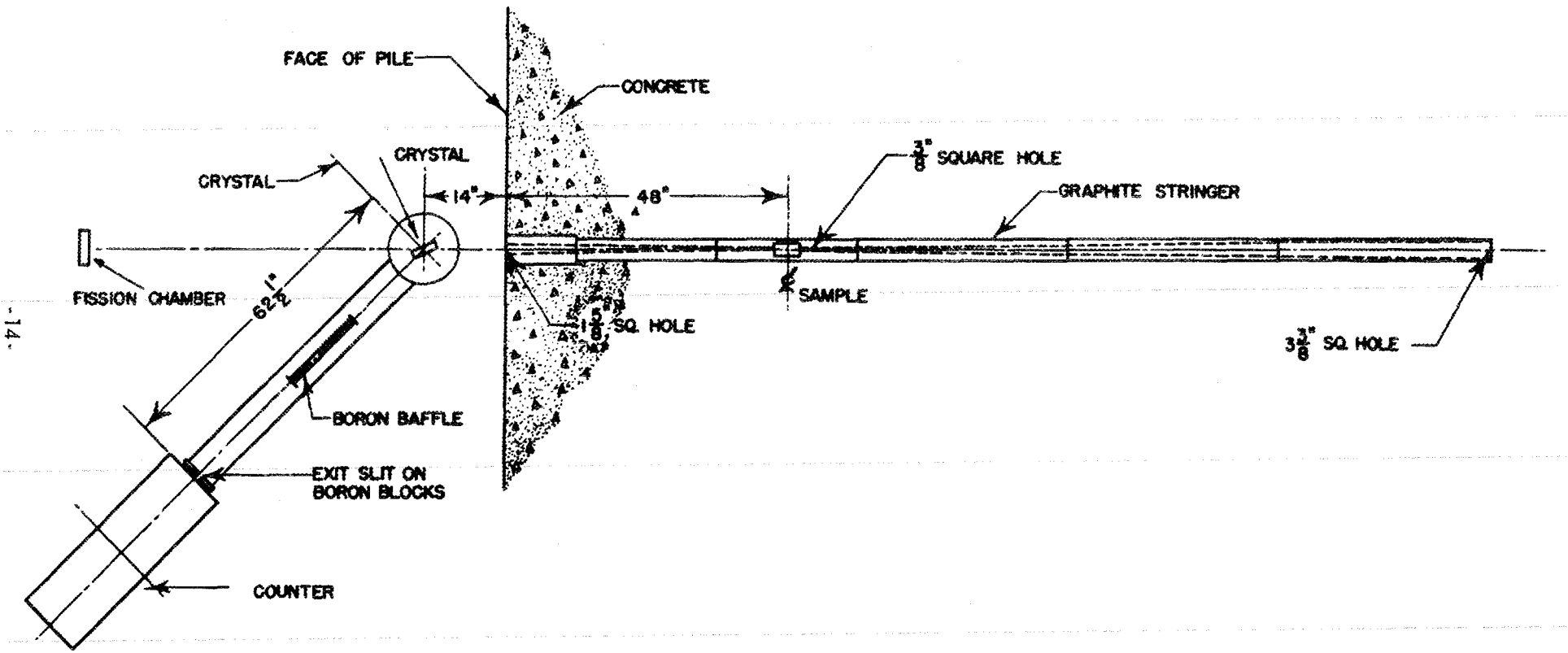

FIGURE 2
NEUTRON SPECTROMETER DIAGRAM

The spectrometer is of the bent crystal type, the curvature of the crystal being adjustable. It can be seen from Figure 2 that the situation is analogous to the Paschen mounting for a concave grating in optical spectroscopy.[3] The sample, about four feet inside the pile shielding, the crystal, and the counter all lie on the Rowland circle.[4] In keeping with the arrangement, the crystal is bent so that its radius of curvature is equal to the diameter of the Rowland circle. In the usual mountings used in optical spectroscopy, the diameter of the Rowland circle is fixed and two of the three elements on the circle are movable. The neutron crystal spectrometer used in this experiment differs from the Paschen mounting in that only one point on the Rowland circle, the dectector, is movable. Thus in selecting a new neutron wave length, it is necessary to move the dectector, to change the angle which the crystal presents to the beam and to change the crystal curvature so that the radius of curvature is equal to the diameter of the new Rowland circle. Each energy setting has a different Rowland circle.

The focussing properties of this type of spectrometer, while good, can not be perfect.[5] Perfect focussing can be achieved only if

---

[3]Francis A. Jenkins and Harvey E. White, Fundamentals of Physical Optics (New York: McGraw Hill Book Company, Inc., 1937), p.167.

[4]Ibid., pp. 166-167.

[5]Arthur H. Compton and Samuel K. Allison, X-Rays in Theory and Experiment (New York: D. Van Nostrand Company, Inc., 1946), p.753.

the crystal is bent so that the atomic planes coincide with concentric circles of radius equal to the diameter of the Rowland circle and ground so that the surface has a radius equal to the radius of the Rowland circle.[6]

Figure 3 illustrates the overall performance of the instrument. It shows results of measurements of the total neutron cross section of cadmium, a substance whose neutron properties have been very thoroughly studied by a variety of methods because of its common use in slow neutron experiments. The figure compares our results with results obtained by Rainwater et al and published in the Reviews of Modern Physics.[7] The fact that our maximum cross section value is the same as the published one suggests that the resolving power of our instrument is as good as theirs. The fact that our determination of the energy at which the maximum of the resonance occurs agrees with the accepted value, checks the accuracy of our absolute energy scale. The full width at half maximum of the cadmium resonance curve is 0.11 e.v. The fact that it was easily possible to trace out this curve with our instrument, suggests that energy differences less than 0.01 e.v. can be readily distinguished by the apparatus in the region of the cadmium resonance, 0.18 e.v.

---

[6] Ibid., pp. 753-754.

[7] H. H. Goldsmith, H. W. Ibser, and B. T. Feld, "Neutron Cross Sections of the Elements," Reviews of Modern Physics, 19:282, 1947.

UNCLASSIFIED
Dwg. 6263

FIGURE 3

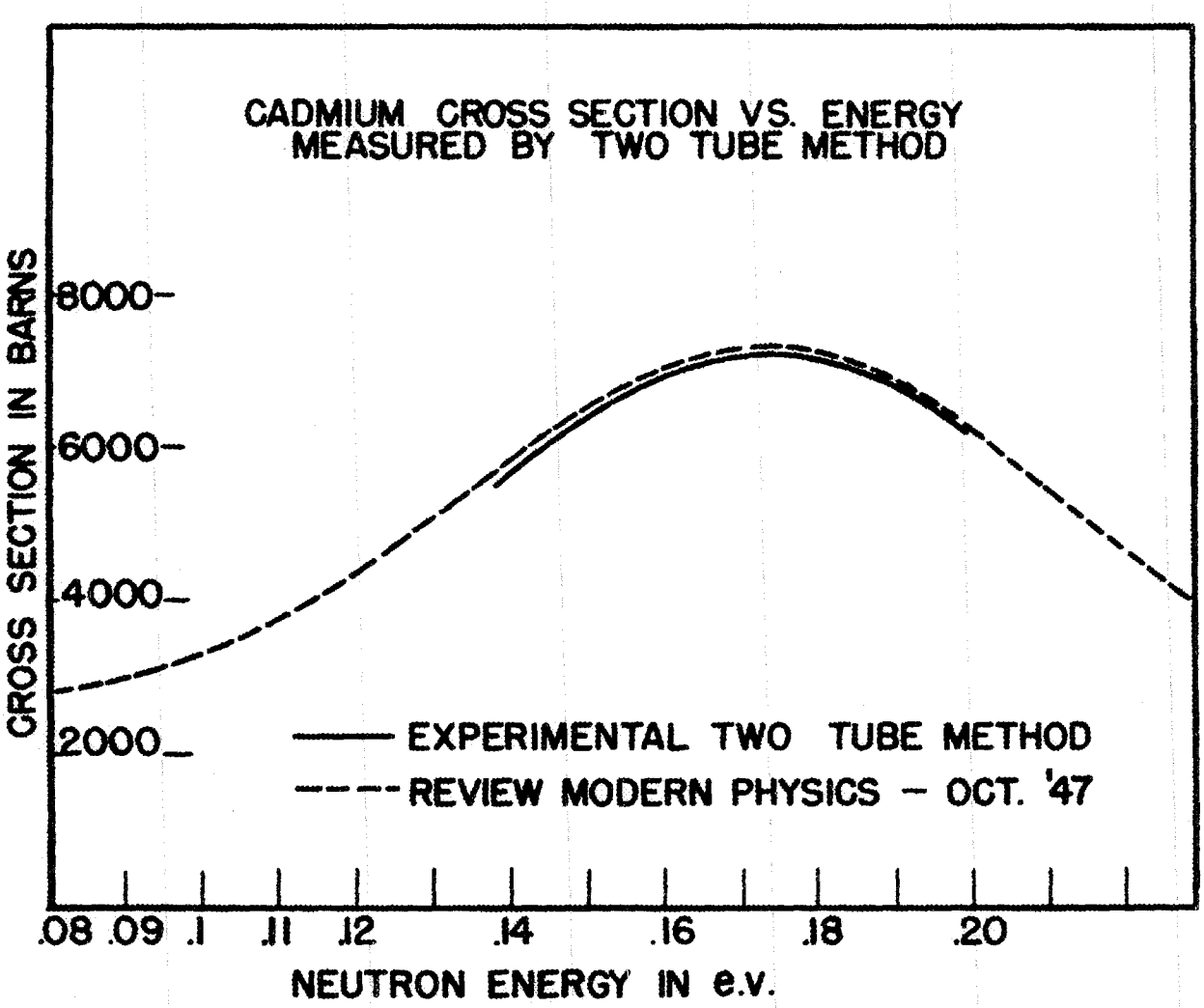

The crystal used is quartz and is five inches by one inch by one millimeter. The crystal is ground so that the 100 planes are parallel to the surface and it is the Bragg reflected beam from these planes which produces the monoenergetic neutrons. The crystal acts as a grating, the distance between the 100 planes being the grating space. The relation between the wave length of the Bragg reflected neutrons and the glancing angle (the glancing angle being the complement of the angle of incidence) is given by Bragg's law.

$$n \lambda = 2 d \sin \theta$$

The formula for the grating space, d, for a hexagonal crystal such as quartz, is[8]

$$d = \frac{1}{\sqrt{\frac{4}{3a_o^2}(h^2 + k^2 + h k) + \frac{\ell^2}{c^2}}}$$

$a_o = 4.9$ angstroms for quartz.[9]

Since it is the 100 planes which produce the Bragg reflection, the Miller indices are $h = 1$, $k = 0$, $l = 0$. Substitution of these values into the above equation gives $d = 4.243$ angstroms.

It is desired to obtain the relation between the energy of the particle and the glancing angle. Since the only case of interest here is for first order reflections, n is set equal to one in the Bragg law:

$$\lambda = 2d \sin \theta$$

---

[8]Martin Buerger, X-Ray Crystallography (New York: John Wiley and Sons, Inc., 1942), p. 103.

[9]Ralph W. Wyckoff, Structure of Crystals (New York: Reinhold Publishing Corporation, 1935), p. 26.

For λ one substitutes the de Broglie wave length, getting

$$\frac{h}{mv} = 2\ d\ \sin\theta$$

Inserting the relation between momentum and kinetic energy into the last expression, $mv = \sqrt{2\ m\ E}$, it follows that

$$2\ d\ \sin\theta = \frac{h}{\sqrt{2\ m\ E}}$$

$$\sin\theta = \frac{h}{2\ d\ \sqrt{2\ m\ E}}$$

Making the appropriate substitutions for the constants, $h = 6.6242 \times 10^{-27}$ erg-sec, $d = 4.243 \times 10^{-8}$ centimeters, and $m = 1.6747 \times 10^{-24}$ grams, gives

$$\sin\theta = \frac{0.4265 \times 10^{-7}}{\sqrt{E}}$$

where E is in ergs. Neutron energies are ordinarily expressed in electron volts. Changing the units of E to electron volts gives

$$\sin\theta = \sqrt{\frac{0.0011359}{E}}$$

This is the relation between the glancing angle, θ, and the energy, E, in electron volts.

Figure 2 shows how the maximum number of neutrons from a 1.5 millimeter source are made to fall on the crystal some five feet away by means of the graphite collimator. At its origin deep in the pile, the beam is 3 - 3/8" x 3 - 3/8" square in cross sectional area. The collimator causes the beam to converge uniformly upon the sample.

The beam is 3 millimeters in diameter when it emerges into the cavity of the graphite stringer section which contains the sample. (See Figures 4 and 5.) Figure 4 shows this graphite stringer section with the sample containing assembly, which is known as the wafer, in place. The neutron beam is here defined by a pyrex glass capillary tube, two inches in length and 1.5 millimeters in diameter. The beam is then allowed to diverge as it leaves the sample, emerges from the pile shielding, and falls upon the bent crystal. Figure 2 shows how the sample is located at the common apex of the two cones of the collimator. In order to test the assumption that the beam was really defined by the boron containing glass, the hole of a capillary tube was plugged with a close fitting boron steel rod and the counting rate of the reflected beam was determined with this arrangement in the incident beam. The counting rate was found to be just equal to the background within 0.03 e.v. to 0.5 e.v., the effective energy range of the instrument.

As stated in the introduction, when taking transmission measurements, it is necessary to count the beam with and without the sample in its path. One might think that it would be much more convenient to have the sample located say at the face of the pile shielding rather than four feet inside that shielding. This is undeniably the case for then it would be a simple matter to place the sample in the beam and to remove it from the beam. One does not always have the luxury of the availability of pure large samples, however, and since the beam is over one inch in diameter when it emerges from the pile, a sample would necessarily weigh several grams. In this particular case somewhat over

UNCLASSIFIED
Photo 4413

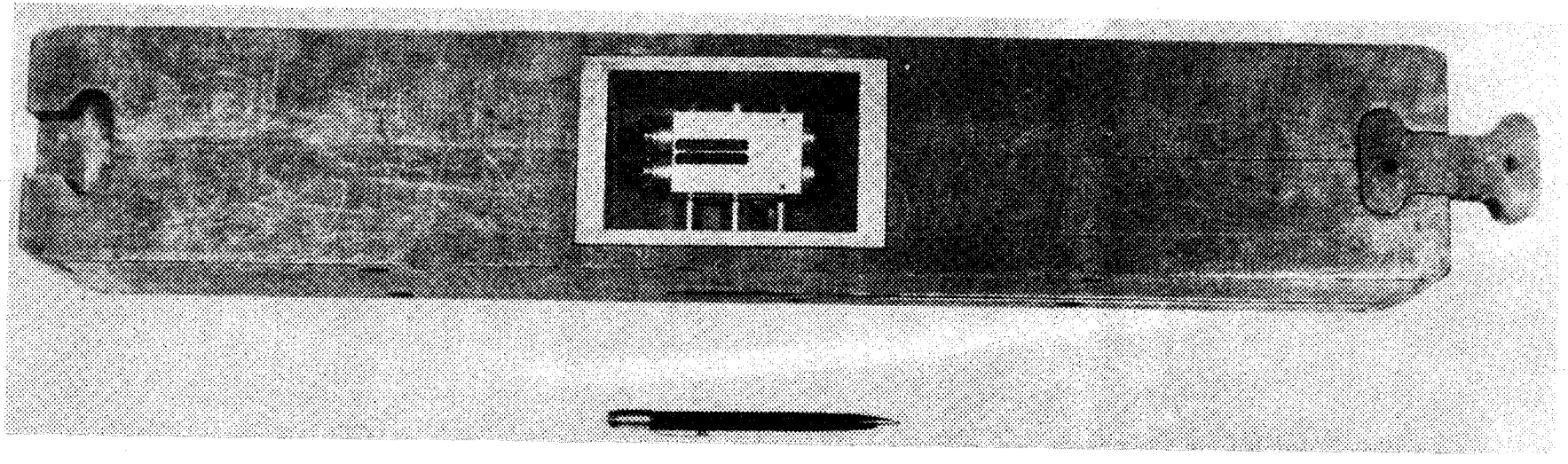

FIGURE 4
SAMPLE SHIFTER SHOWING WAFER IN PLACE

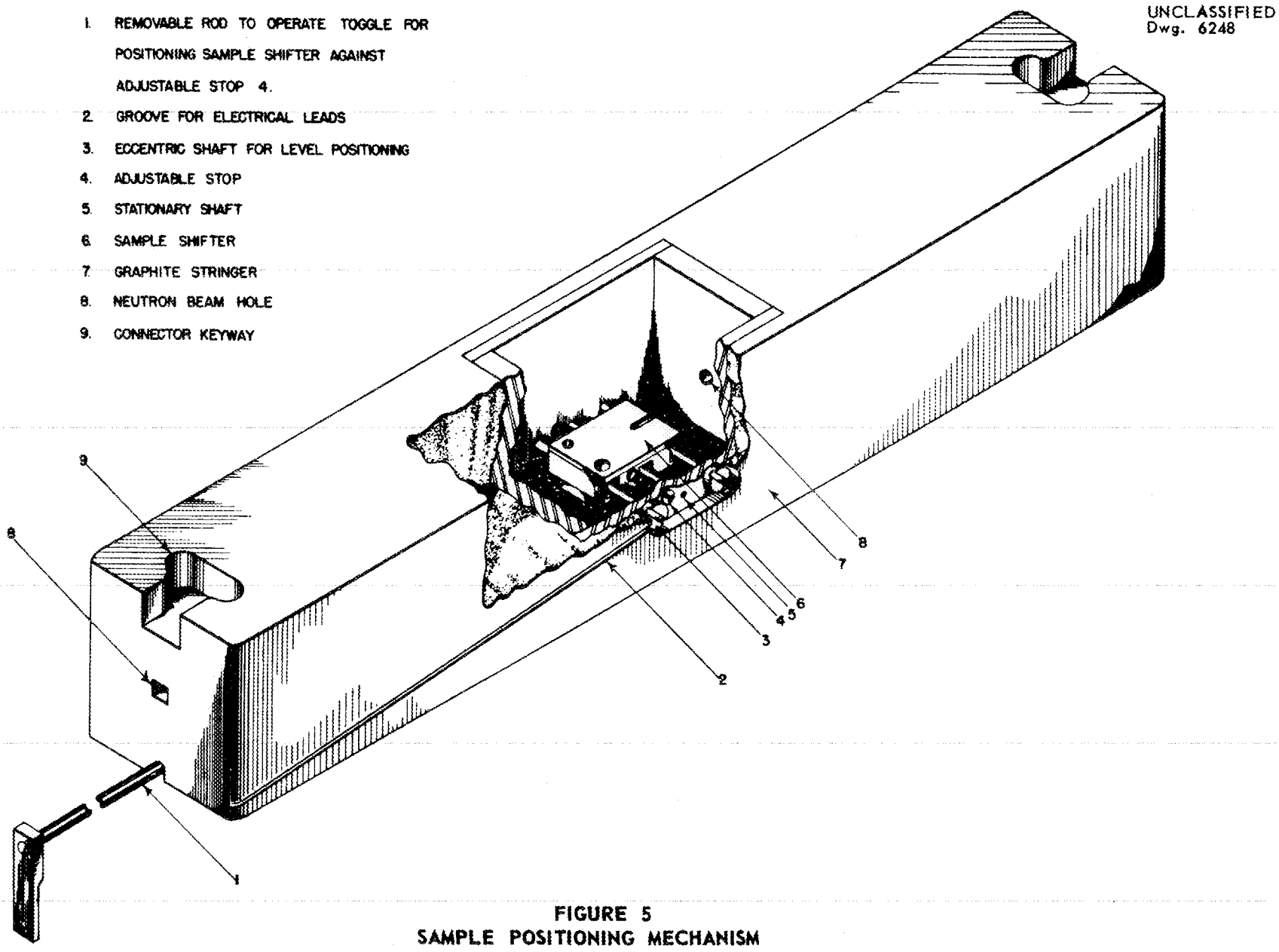

FIGURE 5
SAMPLE POSITIONING MECHANISM

one hundred milligrams of very pure holmium oxide were available. Herein lies the advantage of locating the sample at the apex of the cones of the beam.

The sample shifter (item 6 of Figure 5) of the sample shifting stringer is operated remotely from outside the pile by means of a lever (item 1 of Figure 5) and alternately places either the sample or a blank container in the beam. The requirements placed on the sample shifter are severe. One must be able to shift alternate tubes into the beam repeatedly and get reproducible counting rates through them. It is mandatory that the axes of the two pyrex glass capillary tubes be parallel. The construction of the sample containing assembly, known as the wafer and shown in Figure 6, determines whether the tubes will be parallel or not. It is necessary, therefore, to select a wafer which fulfills this requirement. The apparatus was designed so that the axes of the two pyrex capillary tubes could be adjusted parallel to the axis of the conical collimator hole.

Adjustments available on the sample shifter mechanism are adjustable stops, item 4 of Figure 5, and eccentric shafts for level positioning (item 3 of Figure 5). The wafer or sample containing assembly is shown in Figure 6. It is shown in position on the sample shifter carriage in Figure 4. The bottom view of the wafer in Figure 6 shows the three hemispheres which seat themselves in the matching receptacles of the sample shifter carriage, (item 6 of Figure 5). It also shows the permanent magnet located in the bottom of the wafer, the

UNCLASSIFIED
Dwg. 6247

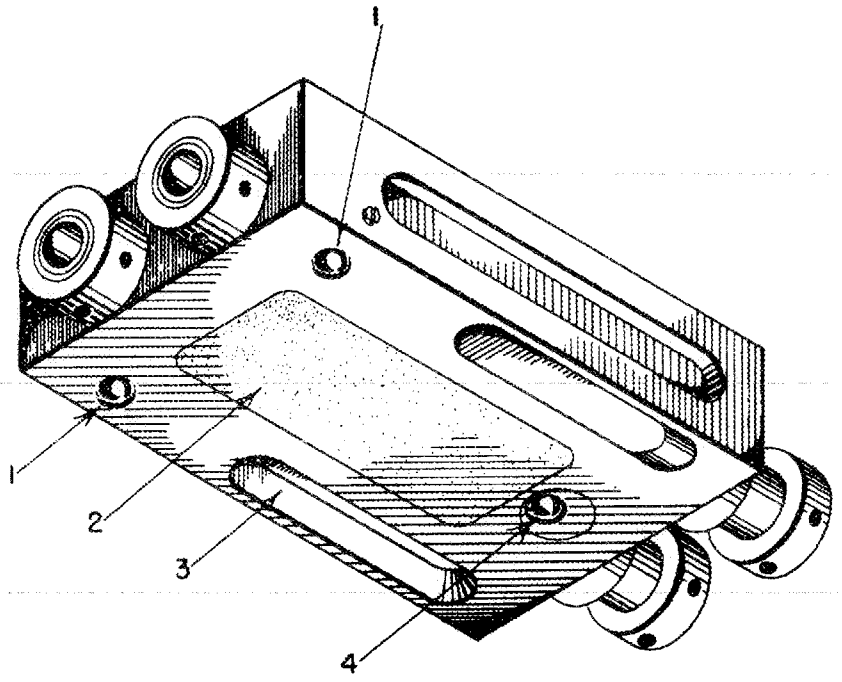

BOTTOM VIEW

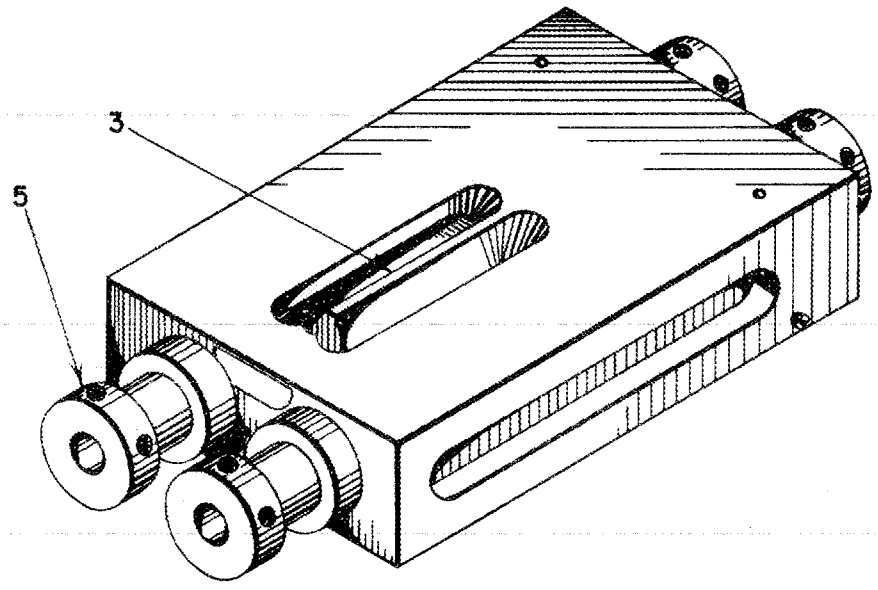

TOP VIEW

LEGEND

1. STATIONARY HALF-BALL
2. MAGNET - ALNICO - V
3. VIEWING SLOT
4. ECCENTRIC HALF - BALL
5. SAMPLE TUBE

FIGURE 6
SAMPLE TUBE HOLDER

purpose of which is to keep the hemispheres seated properly during the shifting operation. Adjustments available on the wafer are first in the vertical direction by means of the two hemispheres labeled item one of Figure 6 and in the horizontal direction by means of the rotable eccentric half ball labeled item 4 of Figure 6. The wafer is made of aluminum and, as shown in Figure 6, holds two parallel brass tubes which house the glass capillary tubes. Figure 7 shows how the sample tube is made up. The pyrex glass capillary tube (item 3 of Figure 7), either empty or containing the sample, is pushed into the brass tube, (item 4 of Figure 7). Koroseal gaskets, (item 5 of Figure 7), seal the ends of the glass capillary tubes. The final seal is made with silicone lubricant applied to the aluminum end plugs, (item 1 of Figure 7), which slip into place in the tapered stainless steel female joint (item 2 of Figure 7).

The most severe test one can make of the performance of the sample shifter is to measure the counting rate ratio for the two tubes in the reflected beam. This has been done many times, the ratio being within the statistical accuracy. Another requirement is that the peak of the rocking curve for one tube should coincide, in angular setting, with the peak of the rocking curve from the other tube. Otherwise the ratio will be far from one, and a small error in angular setting might make reproduction of the ratio impossible so it is desirable to have the rocking curves display flat enough peaks to permit a small error in setting crystal angle, without affecting the

UNCLASSIFIED
Dwg. 6245

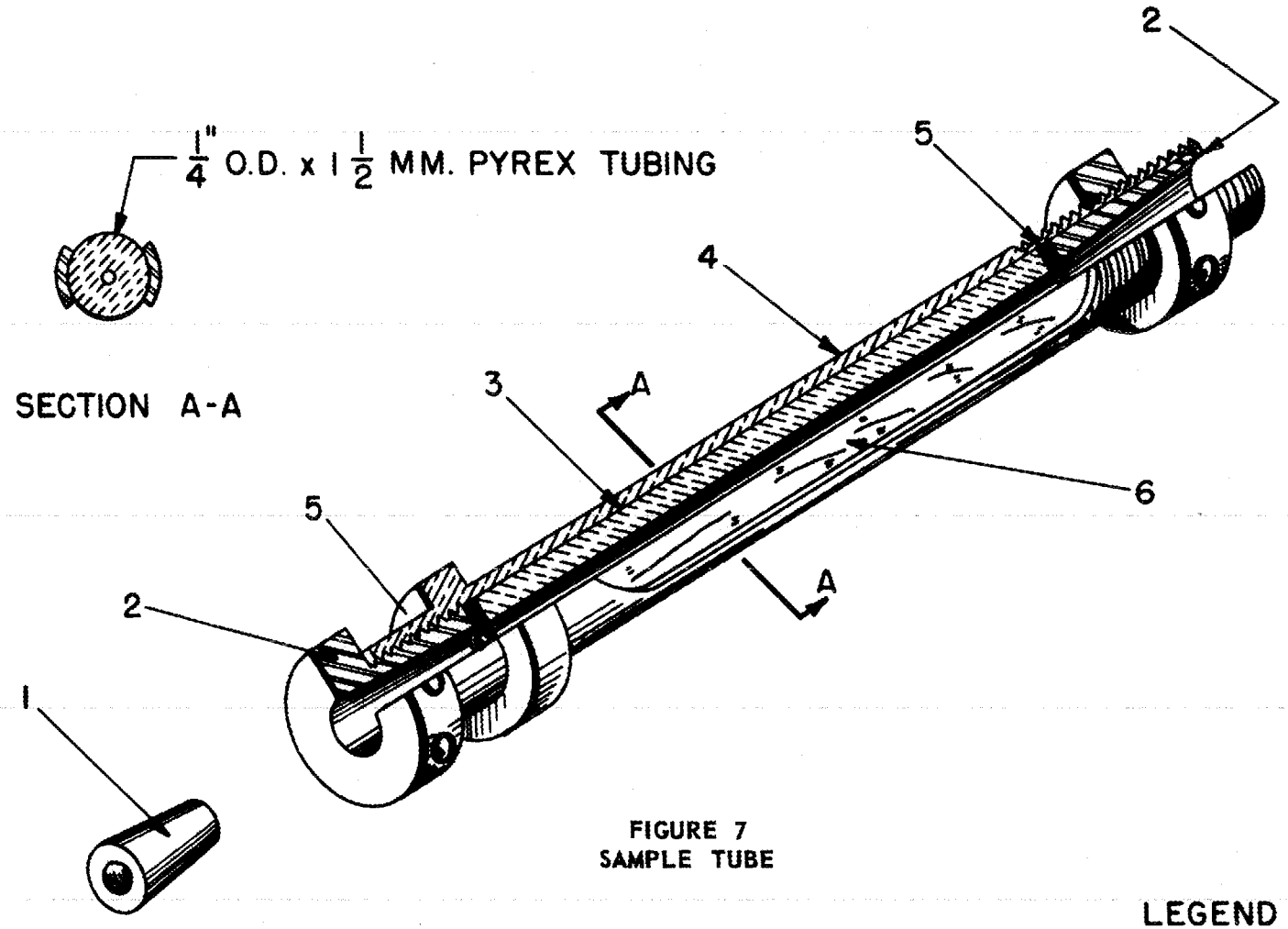

FIGURE 7
SAMPLE TUBE

LEGEND

1. ALUMINUM END PLUG.
2. TAPERED STAINLESS STEEL FEMALE JOINT.
3. PYREX GLASS CAPILLARY TUBE.
4. BRASS ENVELOPE.
5. KOROSEAL GASKET.
6. VIEWING SLOT.

counting rate ratio of the two tubes. The object of the rocking curve is to assure one that the peak of the Bragg reflected beam is being used and it is taken by rotating the crystal until the Bragg peak is established. Figure 8 shows the rocking curves for both tubes and illustrates how the peaks of the two curves coincide and the relative flatness at the top. This flatness was achieved largely by using a six millimeter counter slit rather than a smaller one such as 3 millimeters. The rocking curves were taken by holding the counter angle fixed and rotating the crystal, first with east capillary tube in the incident beam (solid line), and then with the west tube (dotted line) in the neutron beam. Figure 9 is a plot of the counting rate ratio of one tube to the other versus crystal angle. This is usually called the east to west ratio and illustrates the point that, since one can set the circular scale to one minute of arc, there is no need to be concerned about a small error in angular setting causing an error in the east to west ratio. The east to west ratio is important since all measurements made with a sample in one of the tubes must be corrected for the departure of this quantity from unity.

Beginning with Figure 10 are a series of graphs which summarize the performance of the instrument. Figure 10 shows how the counting rate of the crystal reflected beam varies with neutron energy, and Figure 11 shows how the background counting rate varies with energy. Both of these graphs are for a two millimeter source. The reason for the sharp rise in background at about 0.4 e.v. is that the glancing angle is getting quite small ($3^{\circ}\ 3'$) and hence the counter tube is getting close to the primary beam. Figure 12 is a plot of the ratio of

FIGURE 8

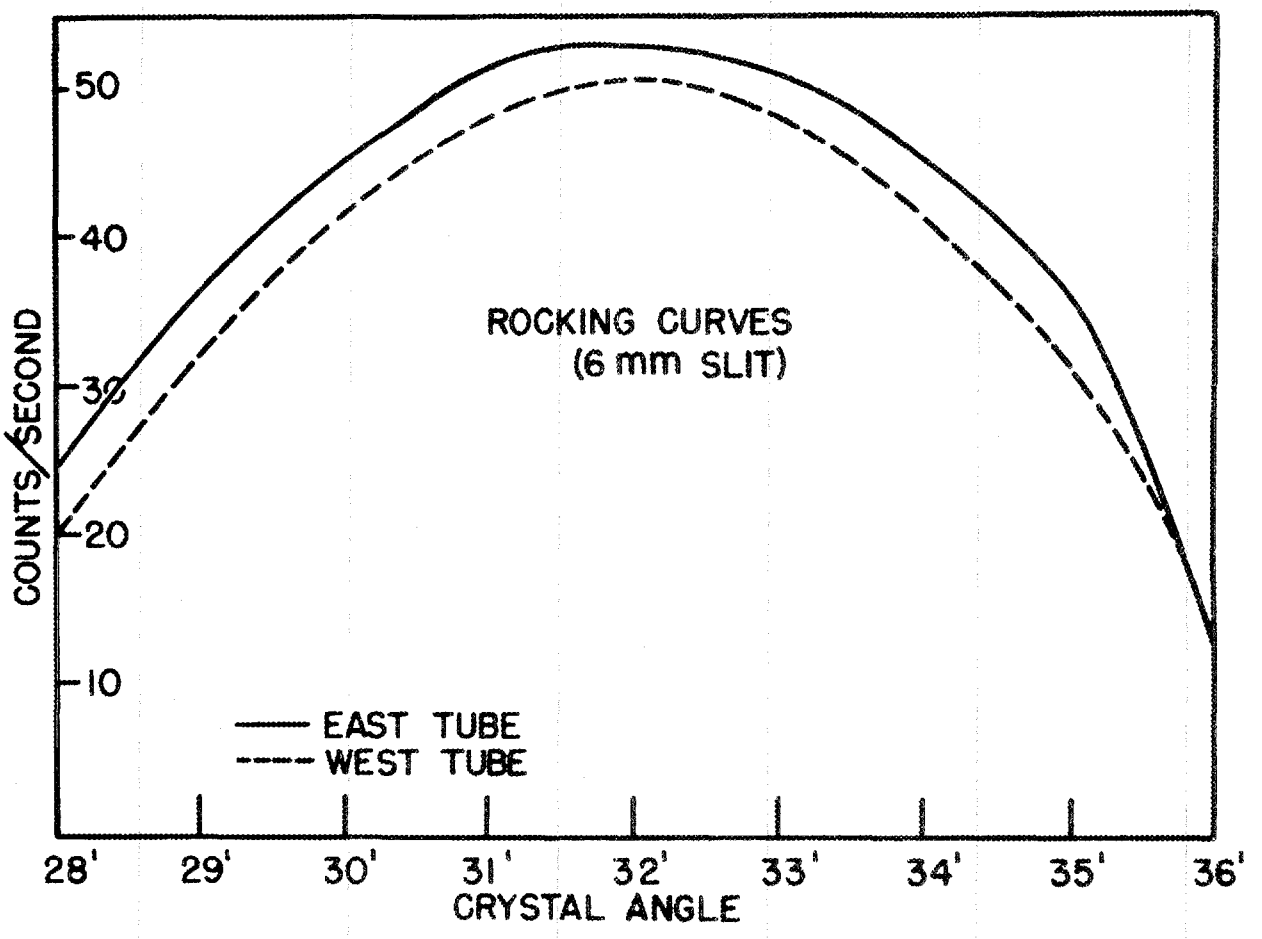
50
40
30
20
10
COUNTS/SECOND
ROCKING CURVES
(6 mm SLIT)
EAST TUBE
WEST TUBE
28'
29'
30'
31'
32'
33'
34'
35'
36'
CRYSTAL ANGLE

FIGURE 9

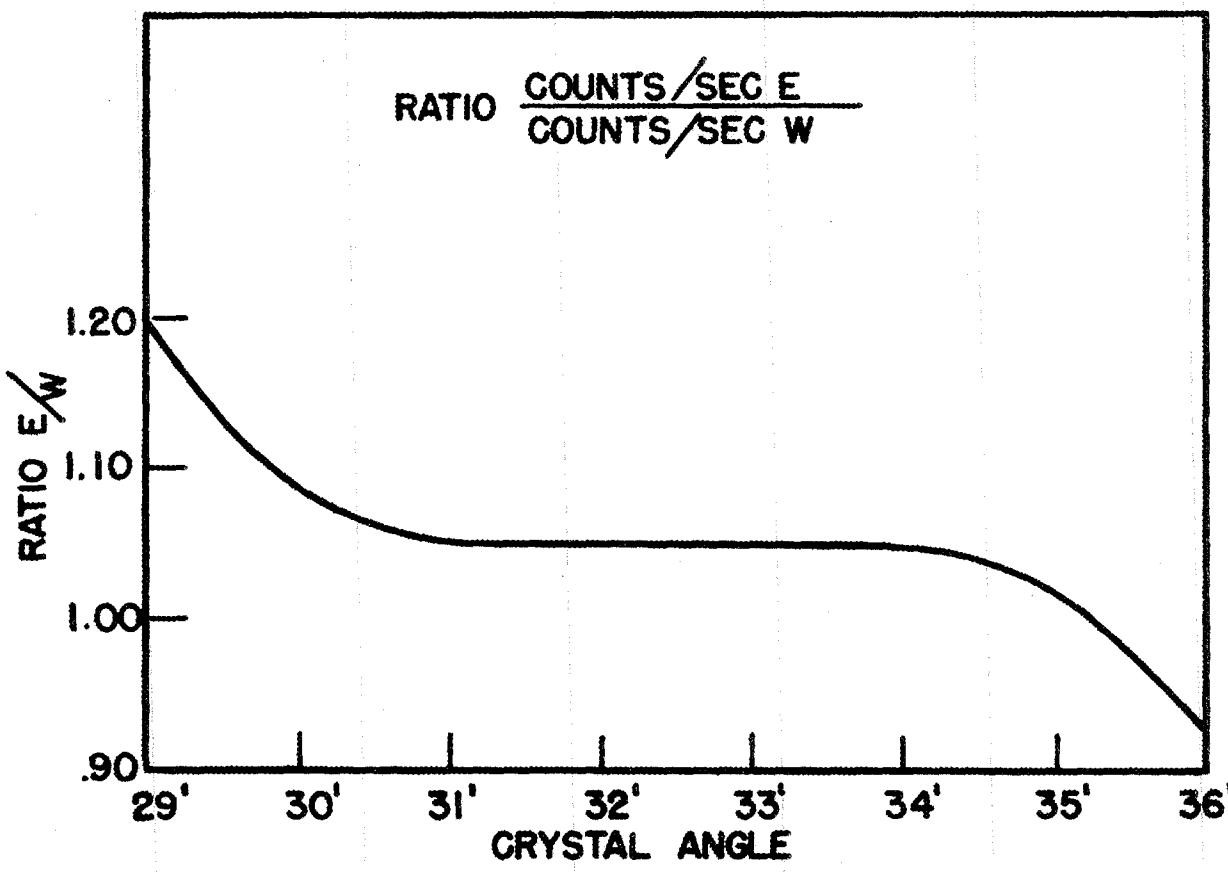
RATIO COUNTS/SEC E / COUNTS/SEC W
RATIO E/W
1.20
1.10
1.00
.90
29'
30'
31'
32'
33'
34'
35'
36'
CRYSTAL ANGLE

FIGURE 10

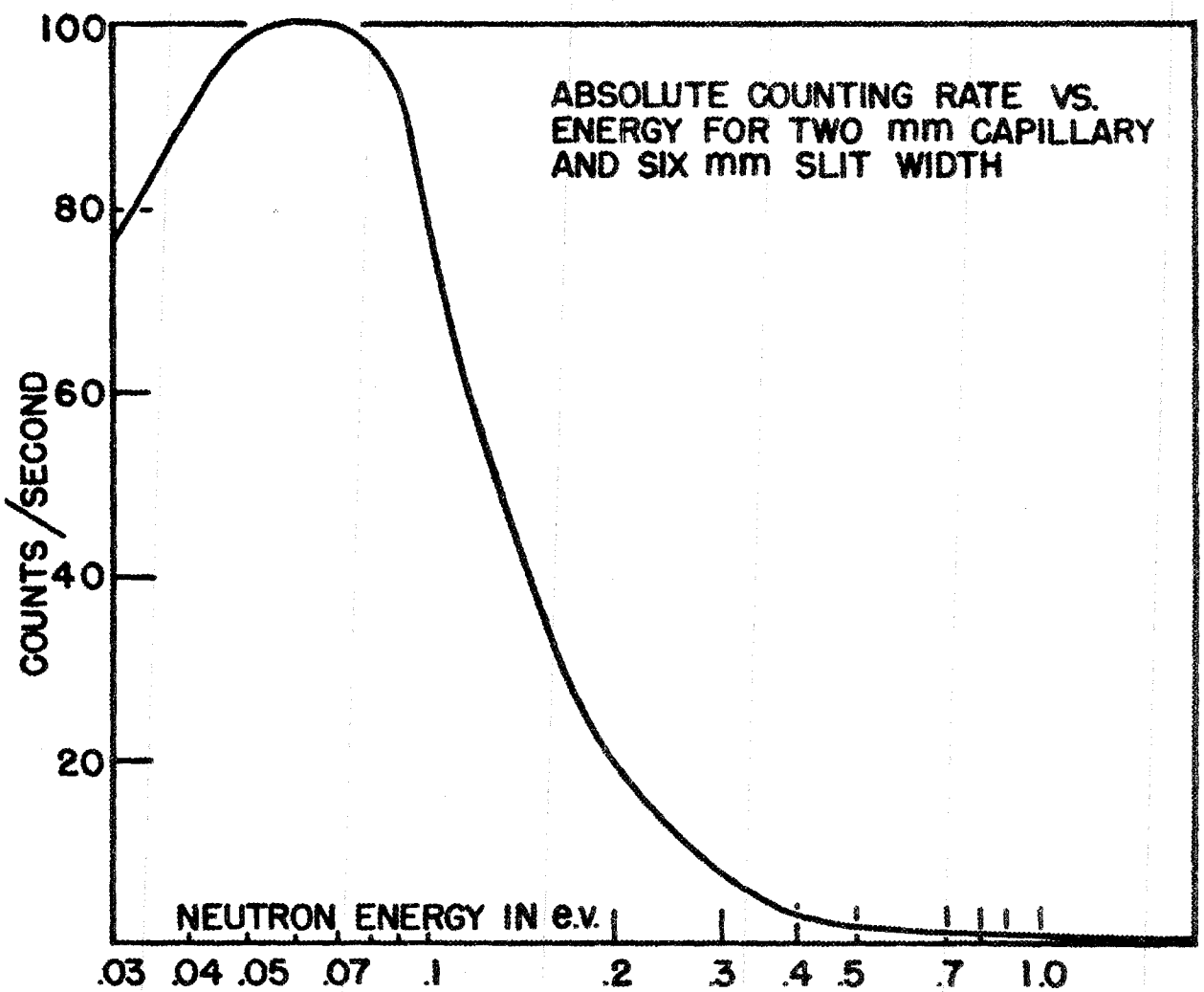
ABSOLUTE COUNTING RATE VS.
ENERGY FOR TWO mm CAPILLARY
AND SIX mm SLIT WIDTH
COUNTS /SECOND
100
80
60
40
20
NEUTRON ENERGY IN e.v.
.03 .04 .05 .07 .1 .2 .3 .4 .5 .7 1.0

FIGURE 11

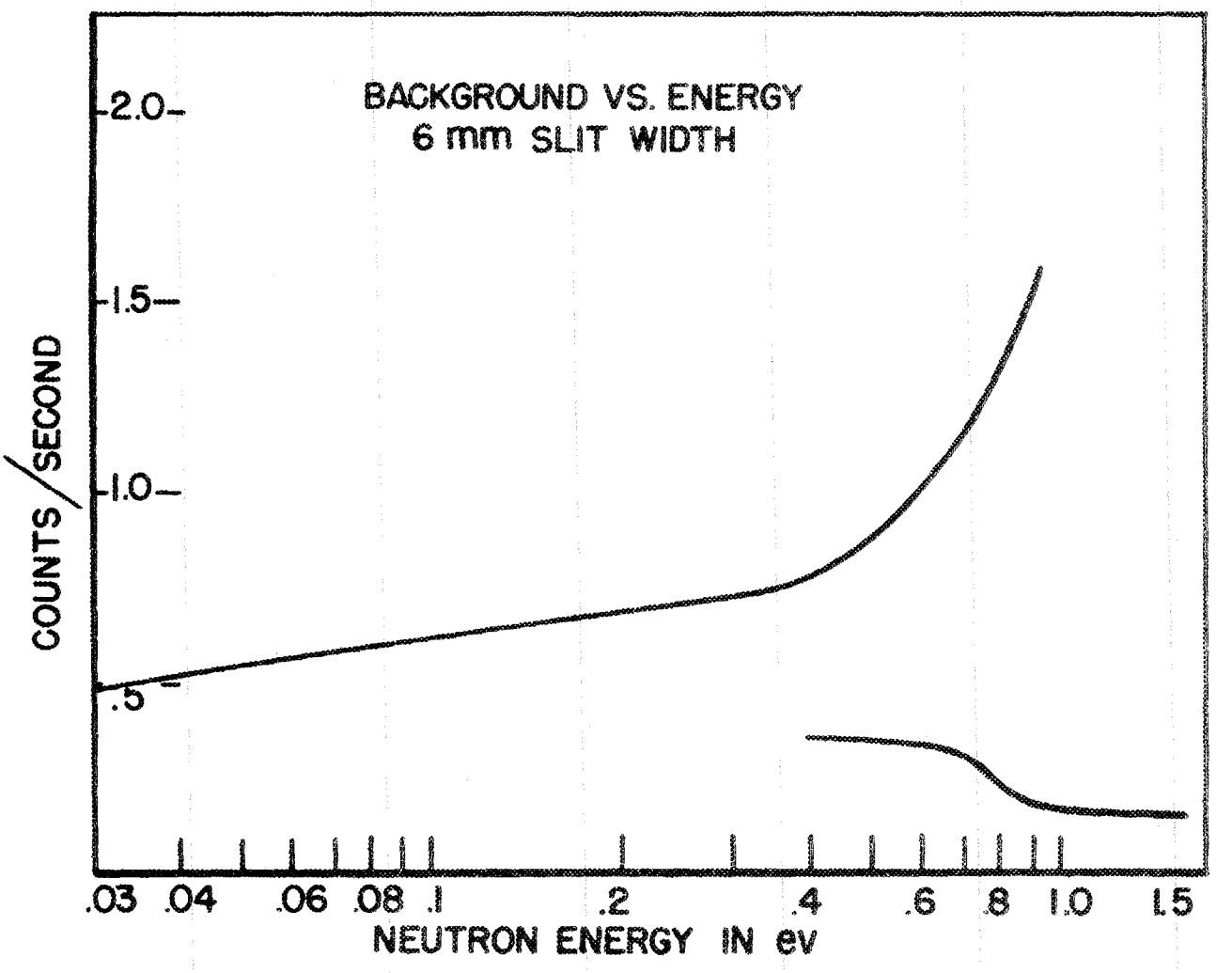
BACKGROUND VS. ENERGY
6 mm SLIT WIDTH
2.0
1.5
1.0
.5
COUNTS / SECOND
.03
.04
.06
.08
.1
.2
.4
.6
.8
1.0
1.5
NEUTRON ENERGY IN ev

UNCLASSIFIED
Dwg. 6266

FIGURE 12

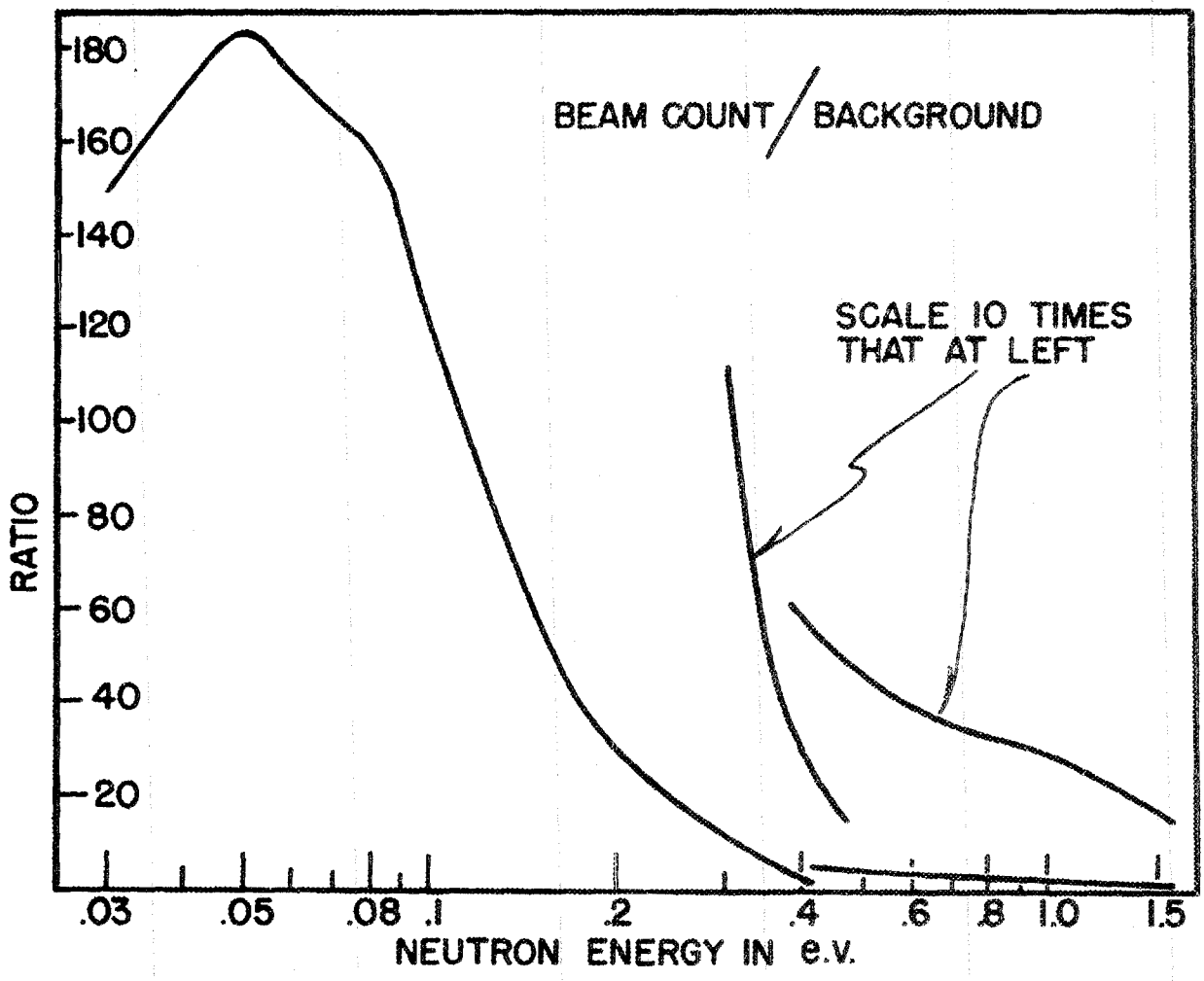

counting rate of the Bragg reflected beam to the background counting rate. The lower curve at higher energies in the last two figures shows how conditions can be improved by using a thin cadmium window over the counter. This improves the beam counting rate to background counting rate ratio at 0.4 electron volts and above for the following reason. Most of the background consists of neutrons of energies below 0.4 electron volts. Cadmium is a strong slow neutron absorber. It has a capture resonance at 0.18 electron volts.[10] The high cross section persists to zero energy but falls off rapidly above .18 electron volts. For example, the cross section at resonance is more than seven thousand barns while at 0.4 electron volts it is about one hundred barns. Consequently, in effect, all neutrons having an energy above a certain "cut-off" are transmitted essentially with no attenuation. The energy 0.4 electron volts is above the "cut-off" and is transmitted preferentially over background neutrons and hence the situation is considerably improved. As one might expect from the two previous curves, the most favorable counting rate occurs at about .05 e.v. and the situation becomes very poor at 0.4 e.v., partly because the background is increasing rapidly here, and partly because the Bragg reflected beam counting rate is rapidly falling off. The variation of counting rate with energy corresponds, of course to the fact that the incident neutron beam is a Maxwell distribution.

---

[10] H. H. Goldsmith, H. W. Ibser, and B. T. Feld, loc. cit.

Proper adjustment of crystal curvature gives optimum focussing and hence maximum counting rate and optimum resolution. Figure 13, which is a plot of counting rate versus crystal curvature, illustrates the sensitivity of counting rate to crystal curvature. While the abscissa is in arbitrary units, one can get an idea of what these units mean in terms of radius of curvature by looking at Table II in the chapter called "Resolution." For example the radius of curvature at 0.026 electron volts is 296 inches while at 0.5 electron volt it has increased to 1300 inches. Figure 14 shows the perfection of focussing. It is a plot of counting rate of the reflected beam from a two millimeter source versus the slit width in front of the BF_3 counter. With perfect focussing the counting rate would have reached a maximum with a slit width of 2 millimeters. Instead we see that it reaches about 80% of maximum at a slit width of three millimeters.

It should be noted that ordinarily transmission measurements are not taken below 0.03 electron volt nor above 0.5 electron volts. The reasons for not going above 0.5 electron volts have already been discussed, i.e., a high background with a decreasing beam intensity. Below 0.03 electron volts the higher order effect becomes appreciable and makes interpretation of results most difficult. For higher orders, n is not equal to one in Bragg's law:

$$n \lambda = 2 d \sin \theta$$

For a given angle, θ_1, and for $n = 1$, $\lambda_1 = 2 d \sin \theta_1$

for $n = 2$, $2\lambda_2 = 2 d \sin \theta_1$

for $n = 3$, $3\lambda_3 = 2 d \sin \theta_1$

FIGURE 13

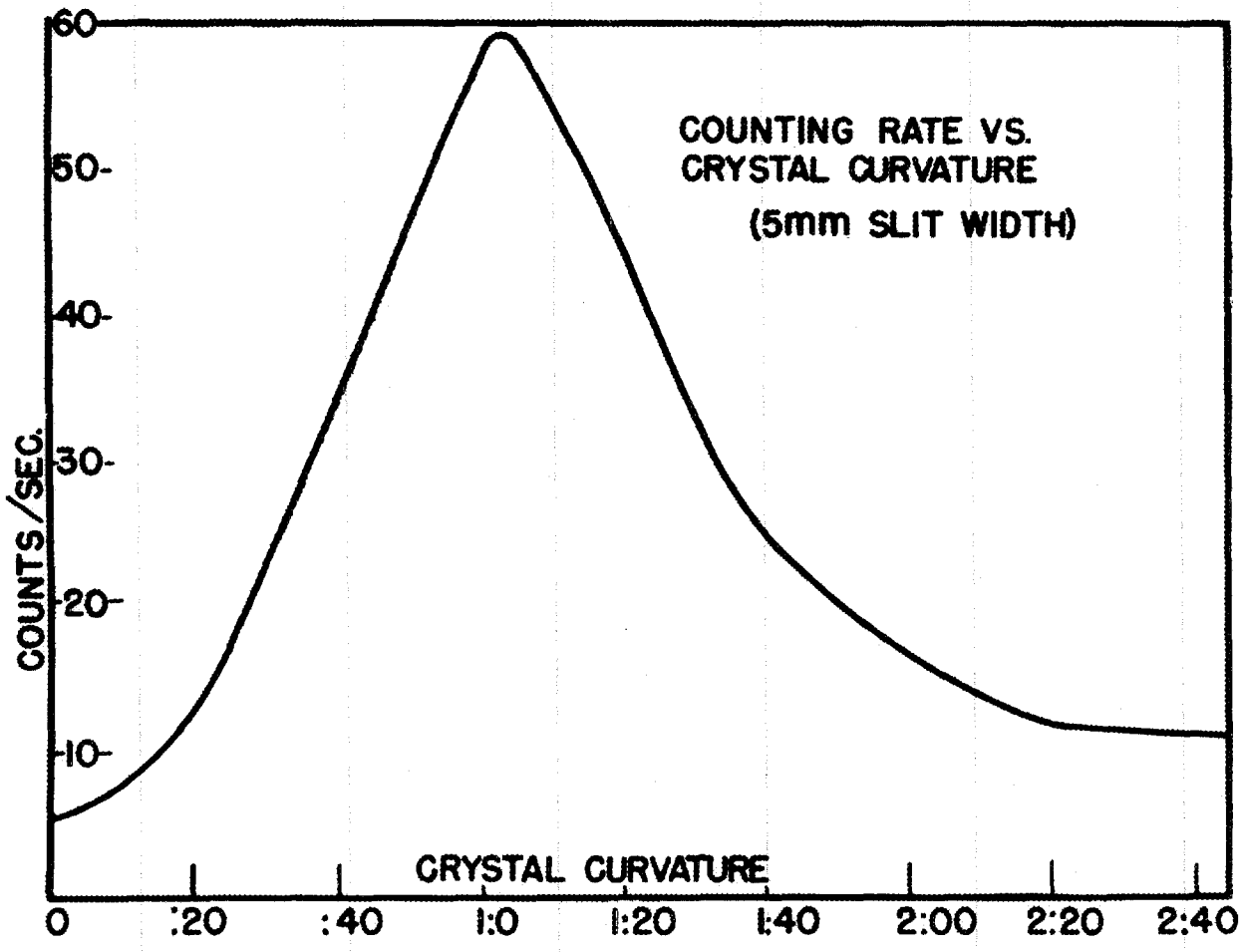
COUNTING RATE VS.
CRYSTAL CURVATURE
(5mm SLIT WIDTH)
COUNTS/SEC.
60
50
40
30
20
10
CRYSTAL CURVATURE
0
:20
:40
1:0
1:20
1:40
2:00
2:20
2:40

FIGURE 14

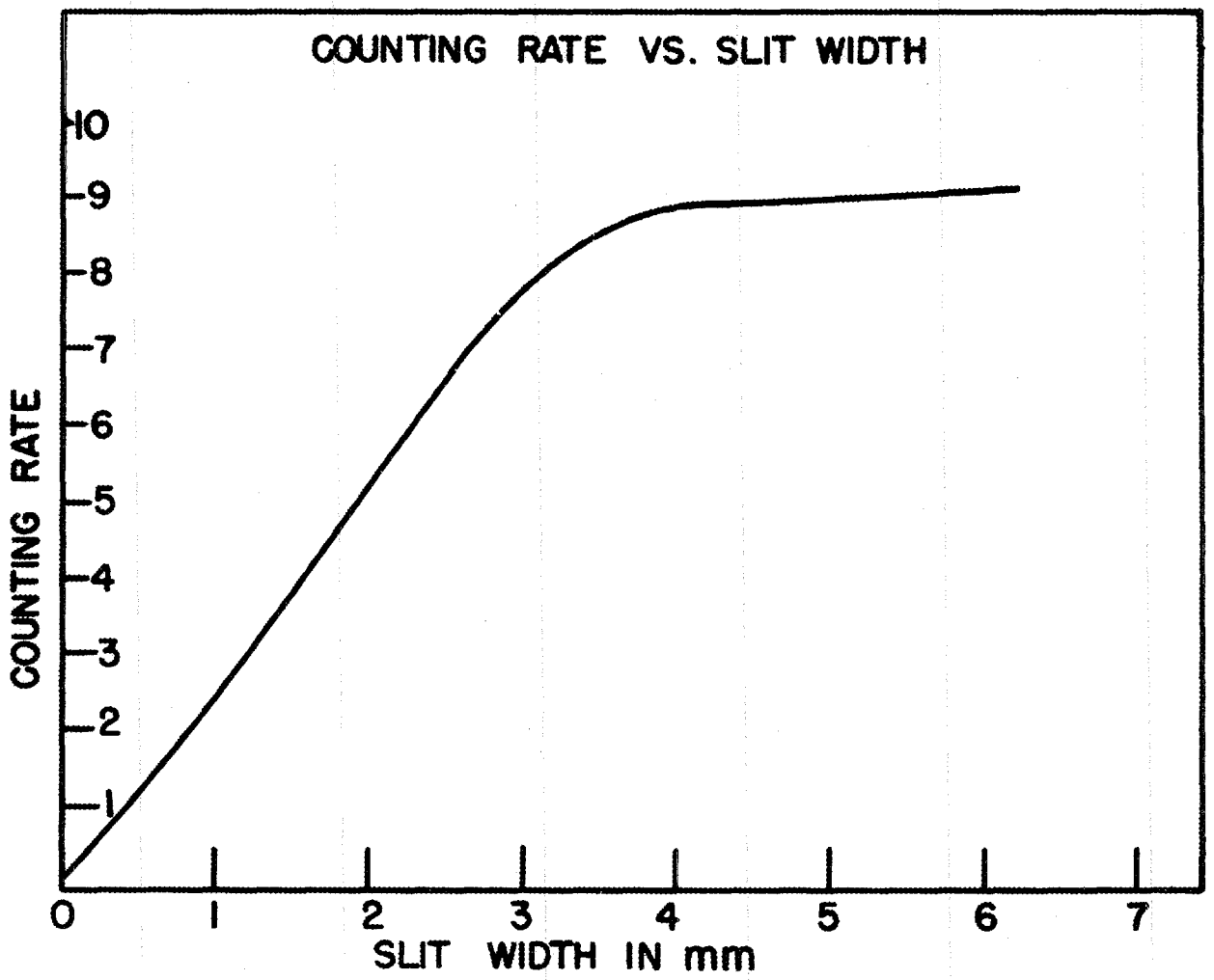
COUNTING RATE VS. SLIT WIDTH
COUNTING RATE
10
9
8
7
6
5
4
3
2
1
0
1
2
3
4
5
6
7
SLIT WIDTH IN mm

In order to satisfy Bragg's law, then,

$$\lambda_2 = \tfrac{1}{2}\ \lambda_1, \text{ and } \lambda_3 = 1/3\ \lambda_1$$

Since wave length is inversely proportional to the square root of the energy, we have:

$$\frac{\lambda_1}{\lambda_2} = \frac{\lambda_1}{\frac{1}{2}\ \lambda_1} = \frac{\sqrt{E_2}}{\sqrt{E_1}}$$

$$E_2 = 4\ E_1$$

Similarly the energy of the third order, E_3, is:

$$E_3 = 9\ E_1$$

Consequently, for a given glancing angle, θ_1, the energies E_1, $4E_1$, $9E_1$, etc. enter the detector. The existence of higher order reflections from the quartz crystal was shown by transmission measurements of boron as a function of energy. When the results are plotted, as in Figure 15, with the negative of the logarithm of the transmission times the square root of the energy versus the energy, one gets a straight line parallel to the energy axis, in the absence of higher orders, since boron is a 1/v absorber. Figure 15 is interpreted, then, as showing that higher order reflections are present below 0.03 e.v. The falling off below 0.03 is caused by the higher order, i.e., higher energy neutrons which are being reflected and thus force one to measure more than one cross section. More precisely, in addition the cross section at the desired energy, one is measuring the cross section at some multiple or multiples

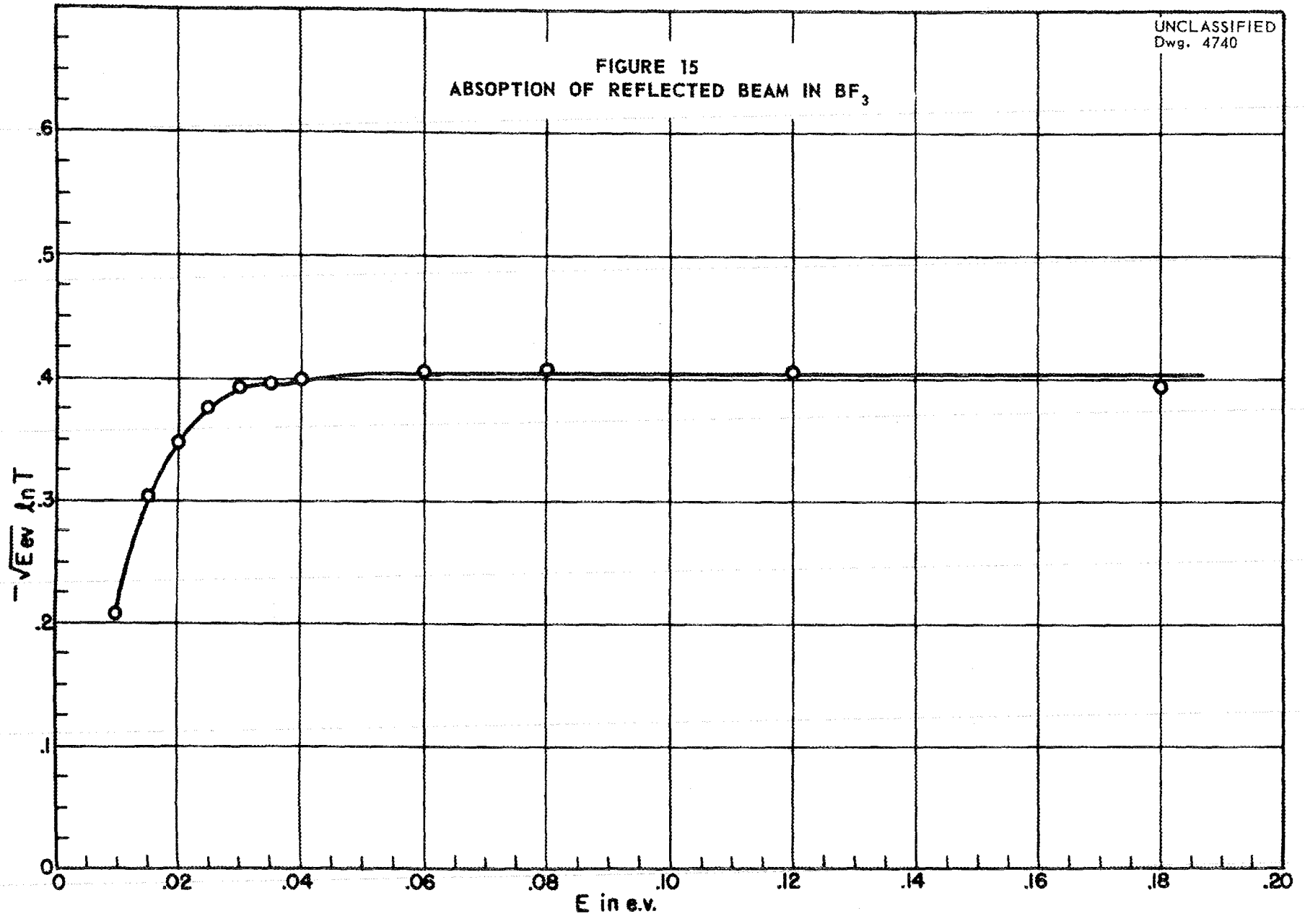
UNCLASSIFIED
Dwg. 4740
FIGURE 15
ABSOPTION OF REFLECTED BEAM IN BF_3
$-\sqrt{E_{ev}}\ \ln T$
0
.1
.2
.3
.4
.5
.6
0
.02
.04
.06
.08
.10
.12
.14
.16
.18
.20
E in e.v.

of this energy. Since the cross section of boron falls off with increasing energy, one observes a smaller cross section when the higher orders are present.

The detector is a boron trifluoride counter, the boron being enriched in the isotope B^{10}. The outer shell of the counter tube is brass. It is about two feet long and two inches in diameter. It is the B^{10} isotope which is responsible for the neutron detection. Neutrons interact with B^{10} as follows:

$$_5B^{10} + {}_0n^1 \rightarrow {}_3Li^7 + {}_2\alpha^4$$

The voltage on the central wire is of such a magnitude (about 1900 volts) that the charge produced by the initial ionization is multiplied by perhaps a factor of 50 during the time that the charge is being collected. The pulses delivered to the grid of the first tube of the four stage preamplifier are proportional to the energy of the α particles produced by the neutrons. A schematic circuit diagram is given in Figure 16.

Before measuring the cross section of a substance, it is necessary to align a wafer and the sample shifter using the adjustments previously described. Then one must take rocking curves for both tubes in order to see if the aligned system satisfies the demands that the peaks of the rocking curves for the two tubes coincide in crystal angular setting. The reasons for this demand have been discussed previously. If this condition is satisifed one then proceeds

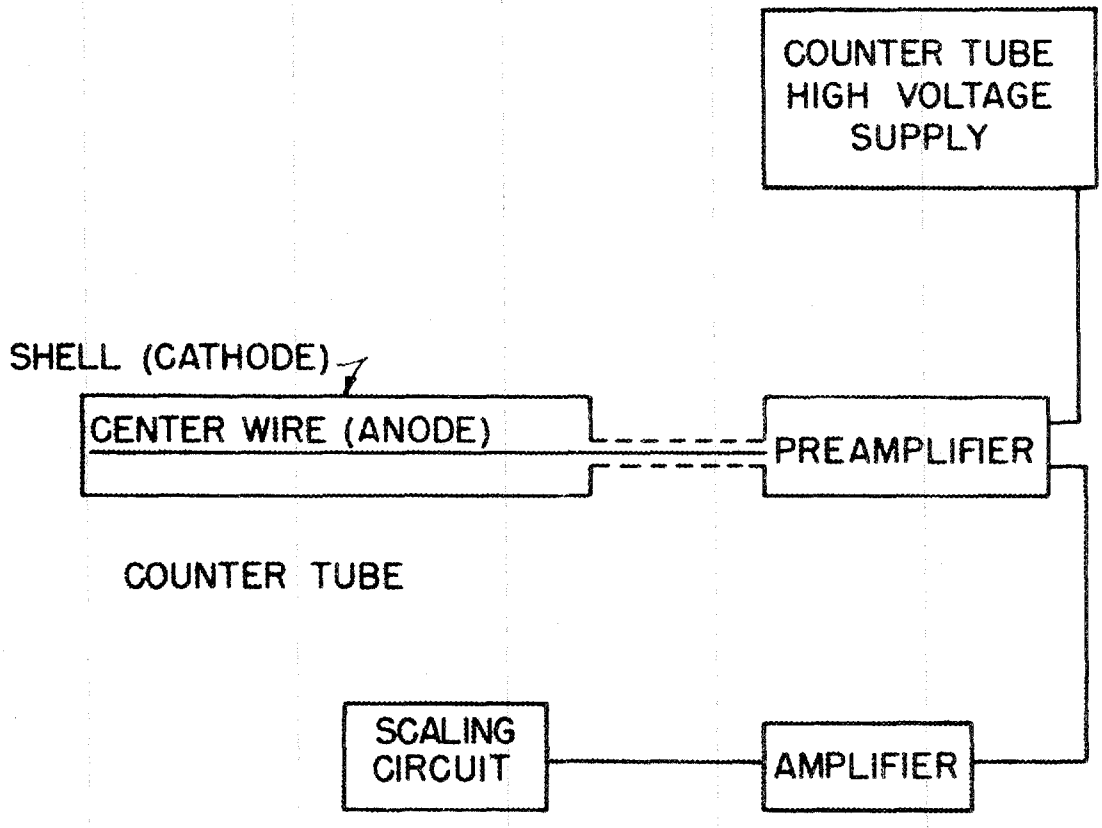

FIGURE 16
SCHEMATIC CIRCUIT DIAGRAM

to measure the counting rate ratio of the two tubes. This is a very important quantity and must be known very accurately, since all measured transmissions for a sample must be corrected for it. When these things have been accomplished, a sample is mounted within one of the capillary tubes and weighed. In taking data, a glancing angle is chosen and the counter angle is adjusted. The crystal is then set on the peak of the rocking curve. Counting rates are then measured with and without the sample in the beam and then background counts are taken for sample in and out of the beam.

In taking background counts one simply moves the crystal thirty minutes from the rocking curve peak, which is more than sufficient to completely erase the Bragg condition. This condition for background measurements is more appropriate than complete removal of the crystal, since it permits taking into account the background caused by incoherent scattering from the crystal and its mounting.

CHAPTER III

RESOLUTION

A calculation has been made of the resolution, based on a Rowland circle geometry. Consideration was first given to the case of a point source. Figure 17 shows a typical Rowland circle. The source, the image, and the center of the crystal, H, all lie on the Rowland circle. The radius of curvature of the crystal is equal to the diameter of the Rowland circle.

It is now desired to know what angular divergence is possible if S is a point source. Referring to Figure 17, θ_1 is the complement of the glancing angle, θ. It is clear that there is a variation in these angles across the grating. Angles S G' C and S H C, which we have called θ_1, and S I' C are equivalent since their vertices lie on the same circle and since all of the angles intercept the same arc length S C. It necessarily follows that angle S G C is less than θ_1 and also that S I C is less than θ_1. This is indicated in the figure by designating angle S G C as $\theta_1 - \Delta\theta_1$ and angle S I C as $\theta_1 - \Delta\theta_1'$. The maximum deviation in θ_1 occurs at the left edge of the crystal, i.e., the edge nearest the source, and all deviations in θ_1 are in the same direction. Note that in the triangles S G J and C H J the angles S J G and C J H are equal since they are formed by intersecting lines. It follows, then, that

$$\angle JSG + \angle JGS = \angle JCH + \angle CHJ$$

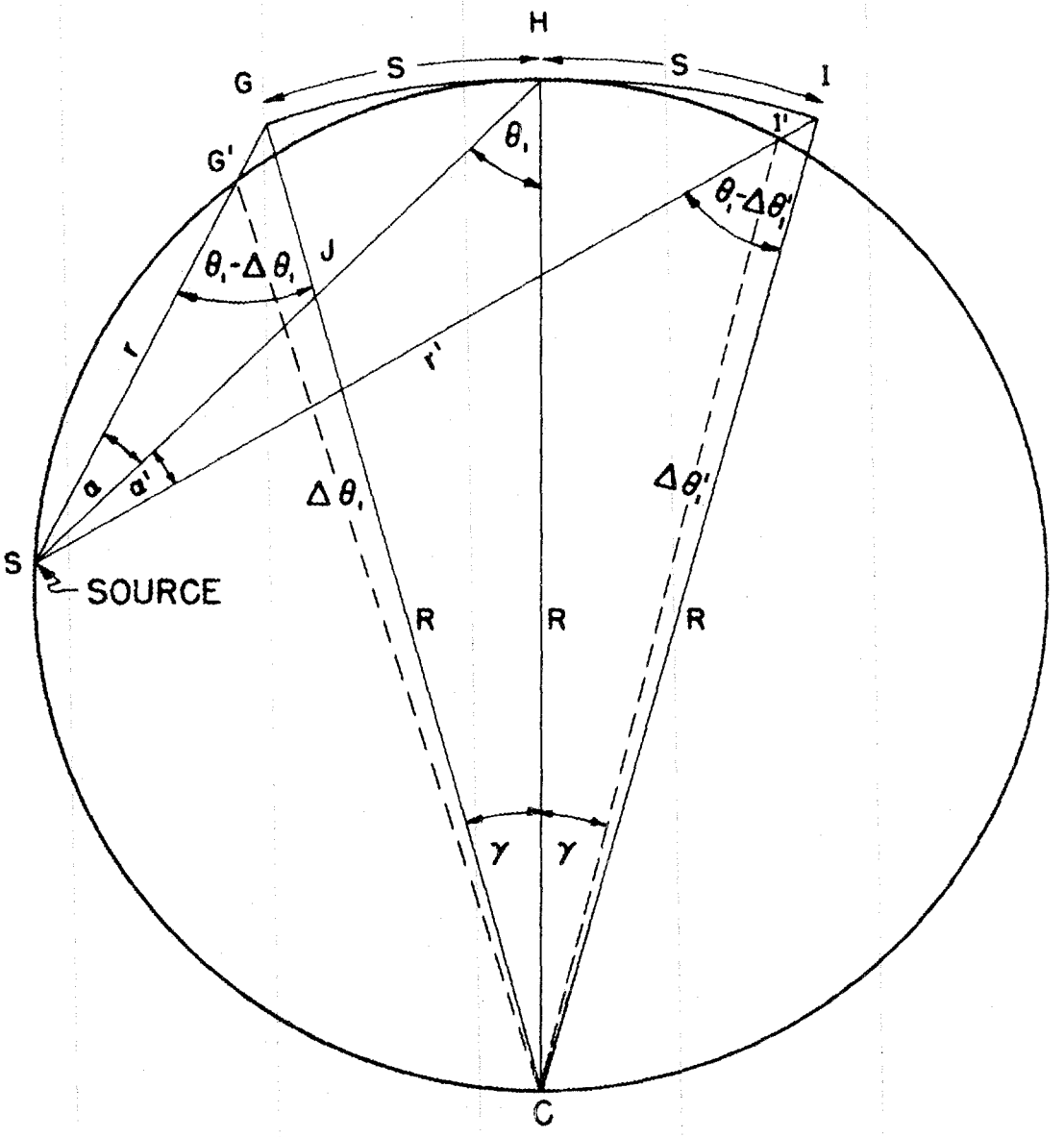

FIGURE 17
THE POINT SOURCE

Using the briefer notation as given in the figure, this equation is:

$$\alpha + \theta_1 - \Delta\theta_1 = \gamma + \theta_1$$

Then $\Delta\theta_1 = \alpha - \gamma$

From the figure $\gamma = \frac{S}{R}$

and α is approximately equal to $\frac{S \sin\theta}{r}$, approximate because the fact that the crystal is curve is neglected. In short α is calculated assuming a flat surface rather than a curved one. The approximation will cause a slight over-estimate of $\Delta\theta$, that is, an upper limit for the value of $\Delta\theta$. This relation also makes use of the approximation, that for small angles the sine of the angle is equal to the angle in radians. Since the maximum value of α is thirty-two minutes, this is a reasonable approximation. (The value of thirty-two minutes in radians is 9.308×10^{-3} and the sin $32' = 9.31 \times 10^{-3}$.)

Therefore

$$\Delta\theta_1 = \frac{S \sin\theta}{r} - \frac{S}{R}$$

This last equation is the variation in glancing angle, and holds at the left edge. S is one-half of the length of the crystal. R is the radius of curvature of the crystal. The distance from the left edge of the crystal to the source is designated by r.

The relation holding at the right edge of the crystal is

$$\gamma + \theta_1 - \Delta\theta_1' = \alpha' + \theta_1$$

$$\Delta\theta_1' = \gamma - \alpha' = \frac{S}{R} - \frac{S \cos\theta_1}{r'}$$

$$\Delta\theta_1' = S\left[\frac{1}{R} - \frac{S \cos\theta_1}{r'}\right]$$

In this equation the distance from the right edge of the crystal to the source is designated as r'.

We must now consider the case of a finite source, namely a source 1.5 millimeters in diameter. It is perhaps most convenient to consider this in four parts corresponding to the four possible situations which give rise to a deviation in glancing angle.

Figure 18 shows one of these situations designated as Case I. Considering the rays as shown, it is clear that the effect of the source is to change θ_1 by a quantity φ and that this quantity φ is in the same direction as was $\Delta\theta_1$ which we have already considered for the point source. A ray striking the center of the crystal from one edge of the source does so at an angle $\theta_1 - \delta$ where δ is equal to the radius of the source divided by the distance from the source to the crystal. The angle corresponding to α of the point source case is larger by a quantity β so that

$$\alpha + \beta = \frac{S \cos(\theta_1 - \delta)}{r}$$

Using the same procedure as before, we have

$$\gamma + \theta_1 - \delta = \alpha + \beta + \theta_1 - \Delta\theta_1 - \varphi$$

$$\Delta\theta_1 + \varphi = \alpha + \beta - \gamma + \delta$$

$$\Delta\theta_1 + \varphi = \frac{S \cos(\theta_1 - \delta)}{r + \Delta r} - \frac{S}{R} + \delta$$

$$\Delta\theta_1 + \varphi = S\left[\frac{\cos(\theta_1 - \delta)}{r + \Delta r} - \frac{1}{R}\right] + \delta$$

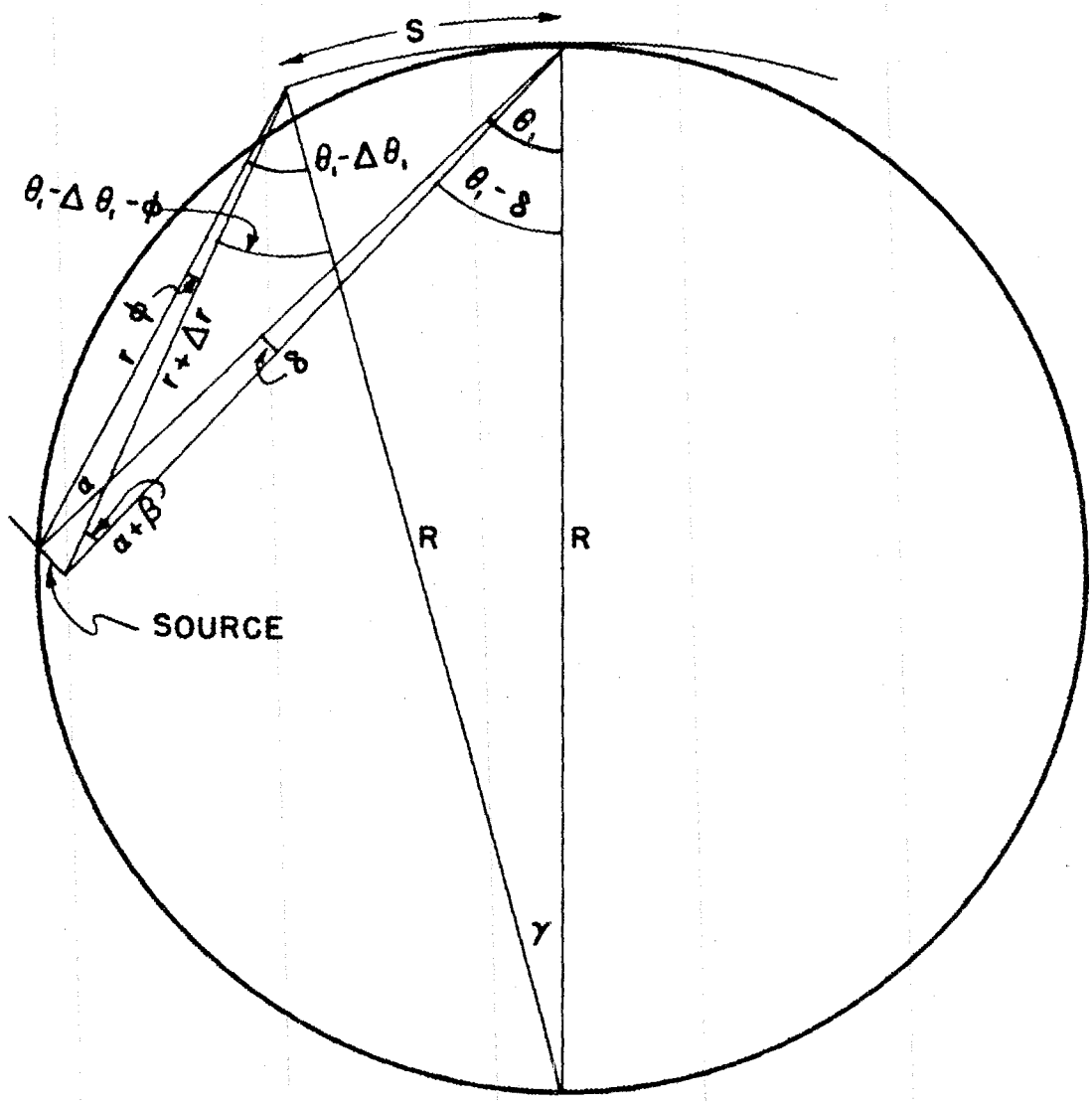

FIGURE 18
THE FINITE SOURCE - CASE I

Figure 19, designated as Case II, shows the situation at the right edge of the crystal, the rays leaving the same edge of the source as before. From the figure we have:

$$\gamma + \theta_1 - \Delta\theta'_1 - \varphi' = \alpha' + \beta + \theta_1 - \delta$$

$$\Delta\theta'_1 + \varphi' = \gamma - (\alpha' + \beta) + \delta = \frac{S}{R} - \frac{S\cos(\theta_1 - \delta)}{r' + \Delta r'} - \delta$$

$$\Delta\theta'_1 + \varphi = S\left[\frac{1}{R} - \frac{\cos(\theta_1 - \delta)}{r' + \Delta r'}\right] + \delta$$

Figure 20, designated as Case III shows the rays leaving the other edge of the source and striking the left edge of the crystal. Proceeding as before, we have:

$$\gamma + \theta_1 + \delta = \alpha - \beta + \theta_1 - \Delta\theta_1 + \varphi$$

$$\Delta\theta_1 - \varphi = \alpha - \beta - \gamma - \delta = \frac{S\cos(\theta_1 + \delta)}{r + \Delta r} - \frac{S}{R} - \delta$$

$$\Delta\theta_1 - \varphi = S\left[\frac{\cos(\theta_1 + \delta)}{r + \Delta r} - \frac{1}{R}\right] - \delta$$

The last situation, shown in Figure 21, gives the following relation:

$$\gamma + \theta_1 - \Delta\theta'_1 + \varphi' = \alpha - \beta + \theta_1 + \delta$$

$$\Delta\theta'_1 - \varphi = \gamma - (\alpha - \beta) - \delta = \frac{S}{R} - \frac{S\cos(\theta_1 + \delta)}{r' + \Delta r'} - \delta$$

$$\Delta\theta'_1 - \varphi = S\left[\frac{1}{R} - \frac{\cos(\theta_1 + \delta)}{r' + \Delta r'}\right] - \delta$$

A sample calculation is given for $\theta = 12^\circ\ 4'$ which corresponds to an energy of 0.026 electron volts.

The first calculation is for the case of a point source.

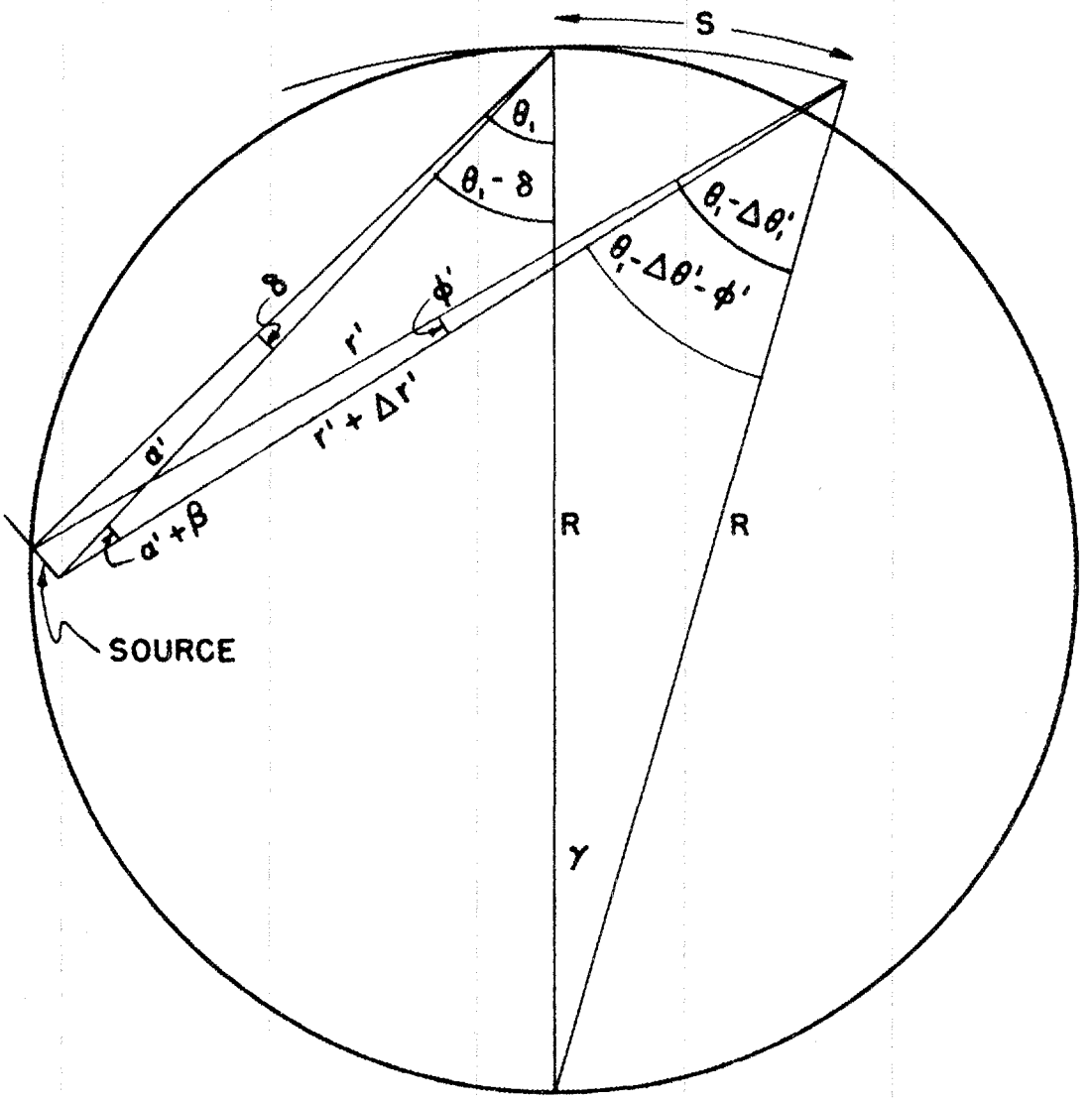

FIGURE 19
THE FINITE SOURCE - CASE II

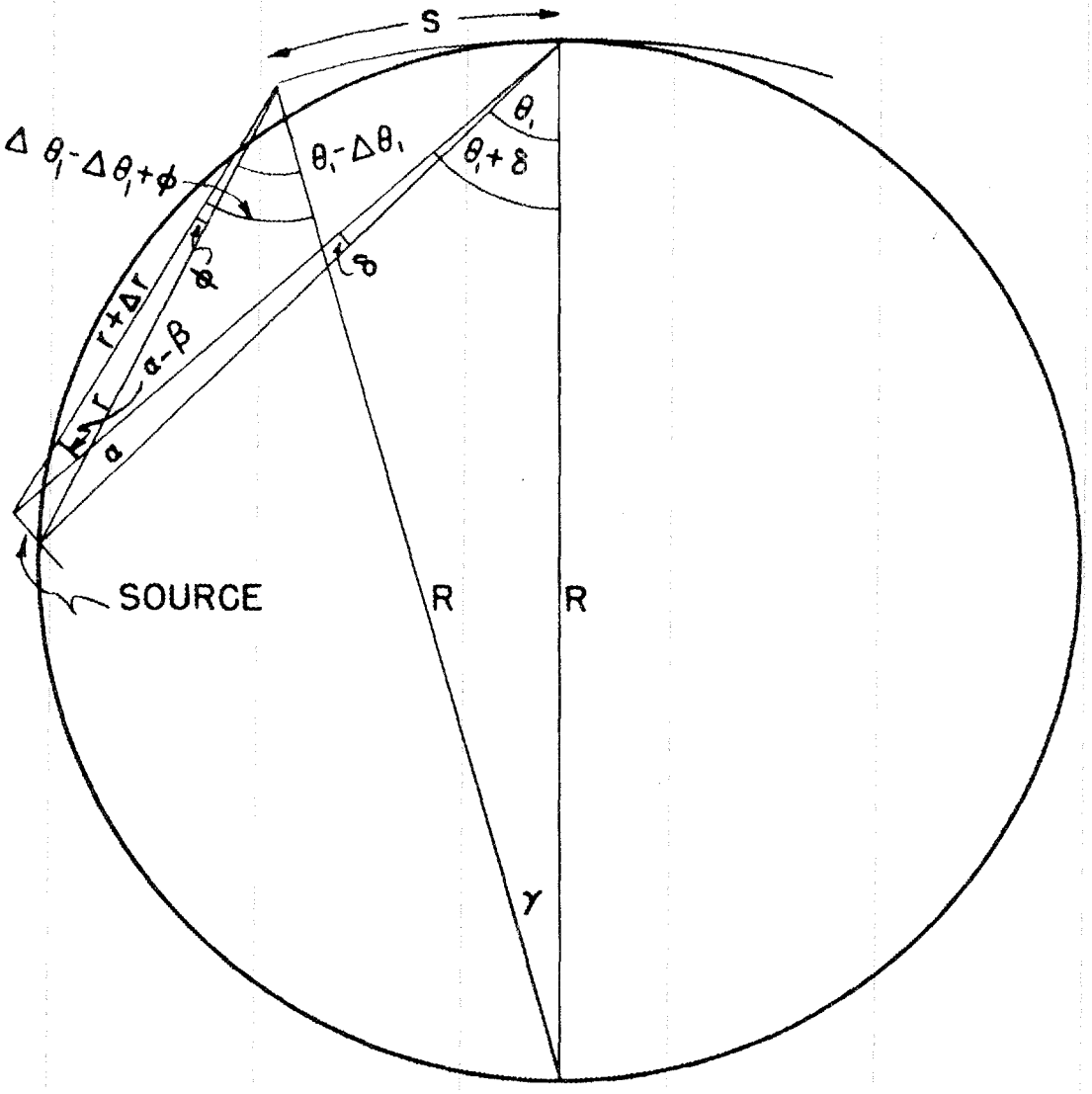

FIGURE 20
THE FINITE SOURCE - CASE III

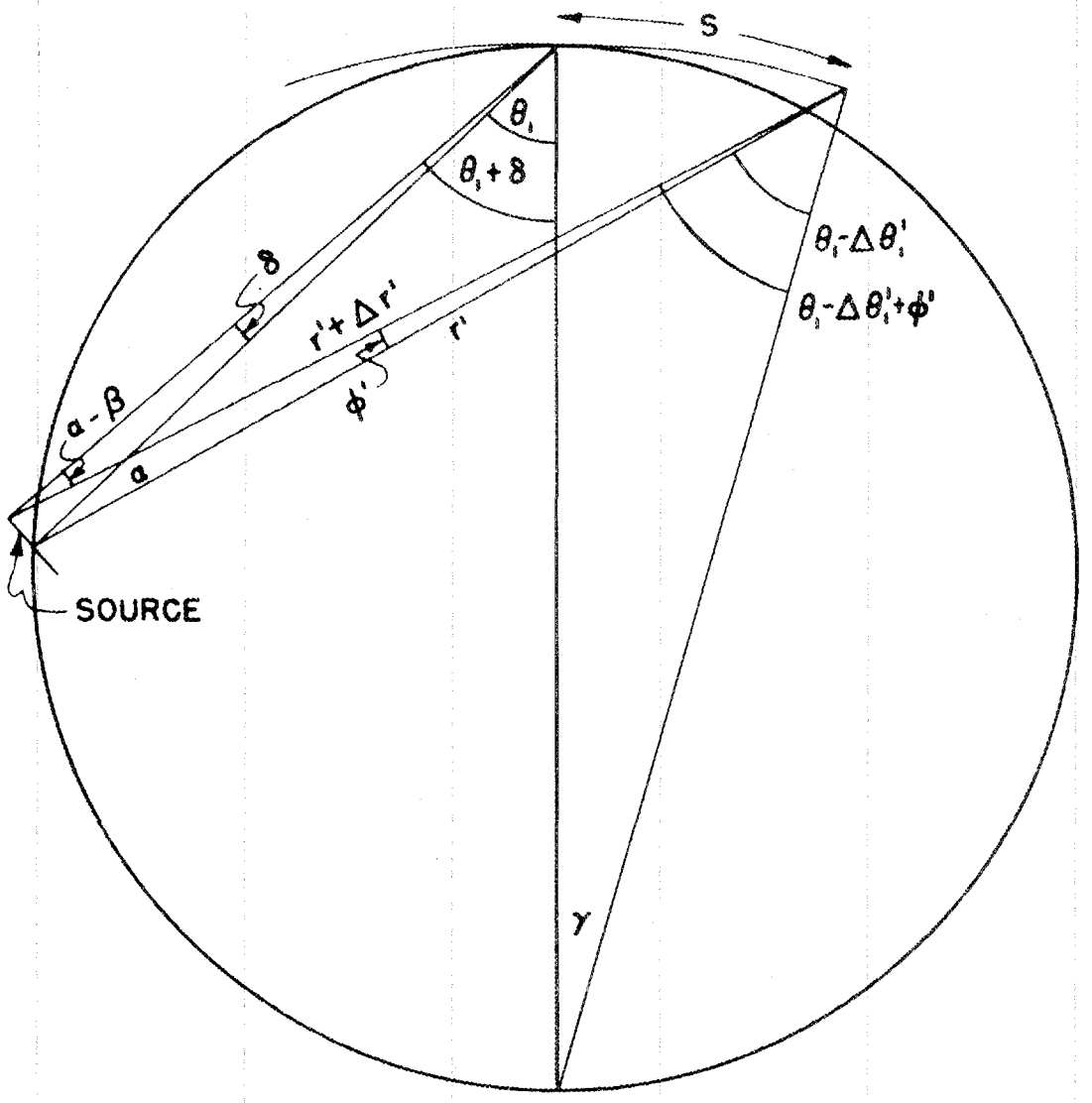

FIGURE 21
THE FINITE SLIT - CASE IV

The maximum deviation in glancing angle at the left edge of the crystal is

$$\Delta\theta = S\left[\frac{\sin\theta}{r} - \frac{1}{R}\right]$$

The value of R, the radius of curvature of the crystal, is, from the geometry of Figure 17:

$$R = \frac{d}{\sin\theta} = \frac{62''}{.20933} = 296''.18$$

where d is the distance from the source to the center of the crystal. The value of r may be obtained by reference to Figure 22a

$$\tan\alpha = \frac{2.5\sin\theta}{62 - 2.5\cos\theta} = \frac{2.5\sin 12^\circ 4'}{62 - 2.5\cos 12^\circ 4'} = \frac{.523325}{62 - 2.4446}$$

$$\tan\alpha = \frac{.523325}{59.5554} = 8.7872 \times 10^{-3} = \sin\alpha$$

$$r = \frac{2.5\sin\theta}{\sin\alpha} = \frac{.523325}{8.7872 \times 10^{-3}} = 59.5554 \text{ inches}$$

By analogy the value of r' is 64.4446 inches. Applying the formula for the left edge, the variation in $\Delta\theta$ is:

$$\Delta\theta = \frac{.523325}{59.5554} - \frac{2.5}{296.18}$$

$$= 8.78720 \times 10^{-3} - 8.44081 \times 10^{-3}$$

$$= 0.34639 \times 10^{-3} \text{ radians} = 1.19 \text{ minutes}$$

and at the right edge the variation is:

$$\Delta\theta = S\left[\frac{1}{R} - \frac{\cos\theta_1}{r'}\right] = \frac{2.5}{296.18} - \frac{.523325}{64.4446}$$

$$= 8.44081 \times 10^{-3} - 8.12054 \times 10^{-3}$$

$$= 0.32027 \times 10^{-3} \text{ radians} = 1.10 \text{ minutes}$$

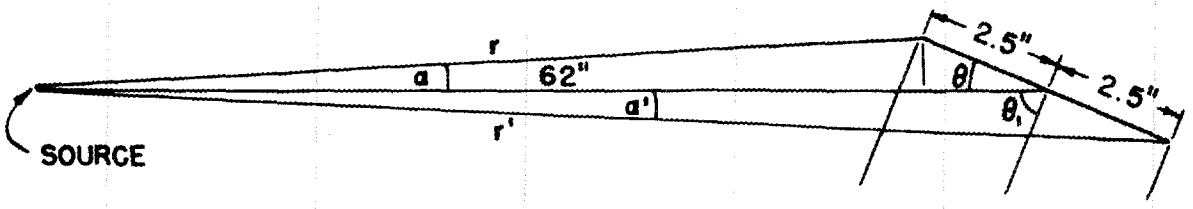

FIGURE 22a
THE POINT SOURCE AND THE CRYSTAL

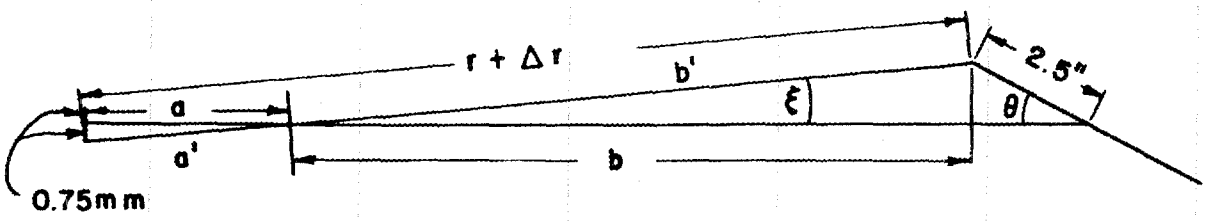

FIGURE 22b
THE 1.5 MILLIMETER SOURCE - CASE I

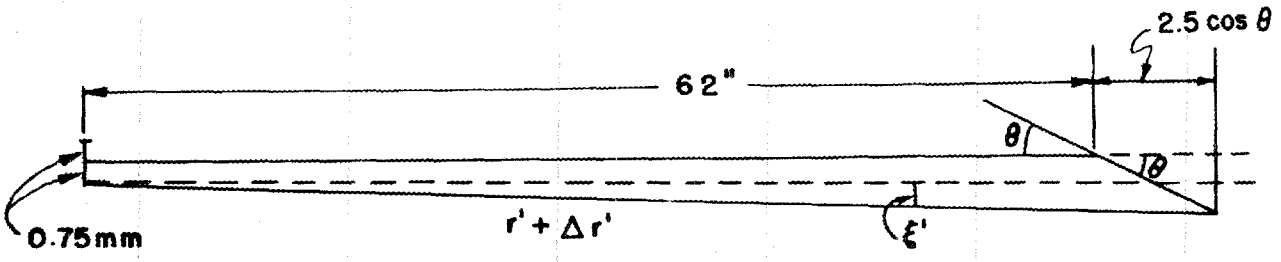

FIGURE 22c
THE 1.5 MILIMETER SOURCE - CASE II

The calculation for the 1.5 millimeter source, Case I, follows. It is necessary to determine the value of $r + \Delta r$ (see Figure 18). By the geometry of Figure 22b, which is also a representation of Case I, we can write:

$$\frac{.075/2.54}{2.5 \sin \theta} = \frac{a}{b}$$

$$a + b = 62 - 2.5 \cos 12^\circ 4' = 62 - 2.4446 = 59.5554$$

Solving these two equations for a and b we get

$$a = 3''.1808$$

$$b = 56''.3746$$

$$\tan \xi = \frac{2''.5 \sin \theta}{56''.3746} = \frac{.523325}{56.3746} = 9.283 \times 10^{-3}$$

$$\xi = 32 \text{ minutes}$$

$$\cos \xi = 0.99996$$

$$a' = \frac{a}{\cos \xi} = \frac{3.1808}{0.99996} = 3.1809$$

$$b' = \frac{b}{\cos \xi} = \frac{56.3769}{0.99996} = 56.3769$$

$$r + \Delta r = a' + b' = 59''.5578$$

Now applying the formula for Case I, we have:

$$\Delta \theta = S \left[\frac{\cos (\theta_1 - \delta)}{r + \Delta r} - \frac{1}{R} \right] + \delta$$

$$= \frac{2.5 \cos (77^\circ 56' - 1''.6)}{59.5578} - \frac{2.5}{296.18} + \frac{.075/2.54}{62}$$

$$= 8.79398 \times 10^{-3} - 8.44081 \times 10^{-3} + 0.47625 \times 10^{-3}$$

$$= 0.8294 \times 10^{-3} \text{ radians} = 2.85 \text{ minutes}$$

At the right edge (Case II) the situation is as pictured in Figure 22c. The value of $r' + \Delta r'$, may be computed as follows:

$$(r + \Delta r)^2 = (62 + 2.5 \cos \theta)^2 + (2.5 \sin \theta - \frac{0.75}{2.54})^2$$

$$r + \Delta r = \sqrt{(64.4446)^2 + (.493797)^2}$$

$$= \sqrt{4153.3503} = 64.4464$$

Now using the formula for Case II, the variation in glancing angle is:

$$\Delta \theta = S \left[\frac{1}{R} - \frac{\cos(\theta_1 - \delta)}{r' + \Delta r'} \right] + \delta$$

$$= 8.44081 \times 10^{-3} - \frac{2.5 \cos(77^\circ 54'.4)}{64.4464} + \frac{.075/2.54}{62}$$

$$= 0.79098 \times 10^{-3} \text{ radians} = 2.72 \text{ minutes}$$

The value of $r + \Delta r$ for Case III, Figure 20, may be obtained by reference to the geometry of Figure 23a.

$$(r + \Delta r)^2 = (62'' - 2''.5 \cos \theta)^2 + (2''.5 \sin \theta - \frac{0.75}{2.54})^2$$

$$= (59''.5554)^2 + (0''.493797)^2$$

$$= 3546''.8456 + 0''.2438 = 3547.0894$$

$$r + \Delta r = 59''.5575$$

Using the formula for Case III, the variation is:

$$\Delta \theta = S \left[\frac{\cos(\theta_1 + \delta)}{r + \Delta r} - \frac{1}{R} \right] - \delta$$

$$= \frac{0.52375}{59.5575} - 8.44081 - 0.47625 \times 10^{-3}$$

$$= -0.12304 \times 10^{-3} \text{ radians} = -0.42 \text{ minutes}$$

The value of $r' + \Delta r'$ for the final case may be obtained from geometry of Figure 23b.

$$a + b = 62 + 2.5 \cos \theta = 64.4446 \text{ inches}$$

$$\frac{a}{b} = \frac{0.075/2.54}{2.5 \sin \theta} = 5.64230 \times 10^{-2} = \frac{a}{64.4446 - a}$$

UNCLASSIFIED
Dwg. 8897

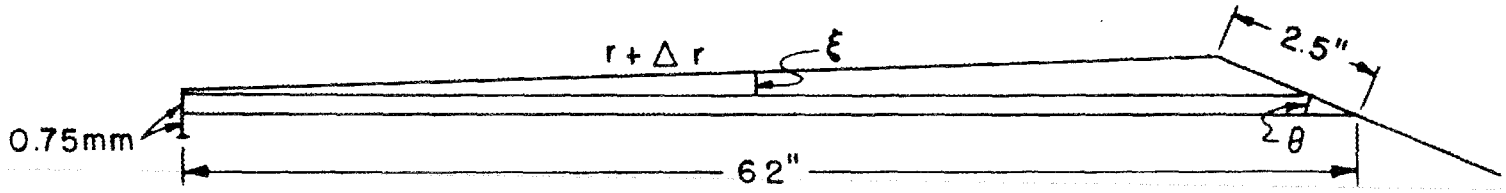

FIGURE 23a
THE 1.5 MILLIMETER SOURCE - CASE III

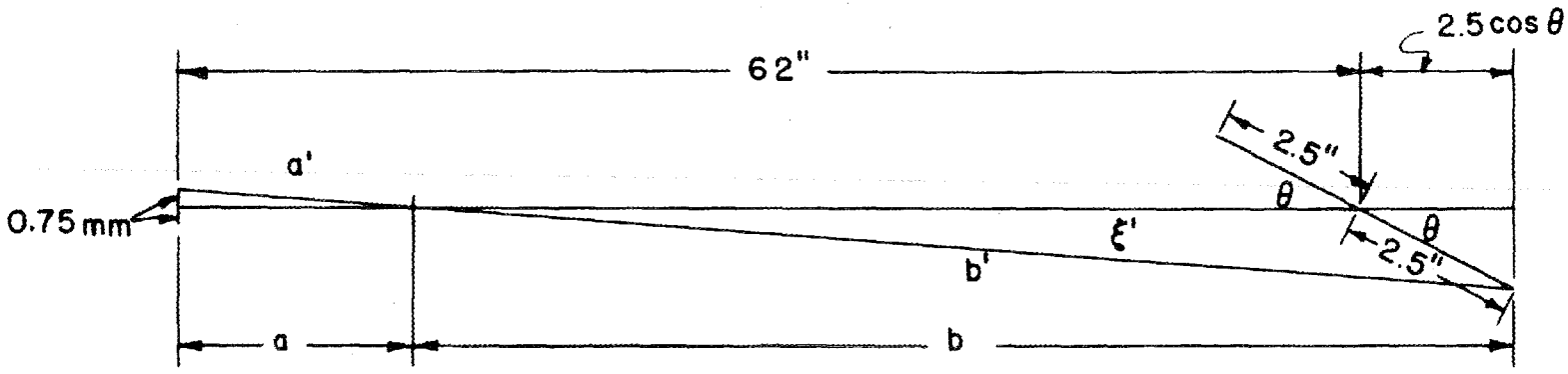

FIGURE 23b
THE 1.5 MILLIMETER SOURCE - CASE IV

$$1.05642\ a = 3.6316$$

$$a = 3''.44196$$

$$b = 61''.00264$$

$$\tan \xi = \frac{0.523325}{61.00264} = 8.579 \times 10^{-3}$$

$$\xi = 29 \text{ minutes}$$

$$b' = \frac{b}{\cos \xi} = \frac{61.00264}{0.99996} = 61.00508 \text{ inches}$$

$$a' = \frac{a}{\cos \xi} = \frac{3.44196}{0.99996} = 3.44210 \text{ inches}$$

$r' + \Delta r' = a' + b' = 64.44718$ inches

Using the formula developed for Case IV (reference Figure 21), the variation is:

$$\Delta\theta = S\left[\frac{1}{R} - \frac{\cos(\theta_1 + \delta)}{r' + \Delta r'}\right] - \delta$$

$$= 8.44081 \times 10^{-3} - \frac{2.5\ (0.20860)}{64.44718} - 0.47625 \times 10^{-3}$$

$$= 8.44081 \times 10^{-3} - 8.0922 \times 10^{-3} - 0.47625 \times 10^{-3}$$

$$= -0.1277 \times 10^{-3} \text{ radians} = -0.44 \text{ minutes}$$

Table I summarizes the results of the above calculations.

In the above considerations, the effect of the slit was not taken into account. The reason for this is that it has no effect on the resolution. The reasons for the wide slit were discussed under Apparatus and Procedure. If the focussing were perfect the size of the image would be the same as the source, i.e., 1.5 millimeters. The image is larger, however, due to the imperfection in focussing. For example the spread in the image at E = .026 electron volts will be:

TABLE I

VARIATION IN GLANCING ANGLE FOR $\theta = 12^\circ\ 4'$

Source	Left Side of Crystal	Right Side of Crystal
Point Source	1'.19	1'.10
1.5 Millimeter Source Cases I and II	2.85	2'.72
1.5 Millimeter Source Cases III and IV	- 0'.42	- 0'.44

$$(\Delta\theta \text{ at left edge})\ (64.45)\ (2.54)\ (10)$$
$$+ (\Delta\theta \text{ at right edge})\ (59.56)\ (2.54)\ (10)$$
$$= (0.8294 \times 10^{-3})\ (64.45)\ (2.54)\ 10$$
$$+ (0.1277 \times 10^{-3})\ (59.56)\ (2.54)\ 10$$
$$= 1.36 + 0.19 = 1.55 \text{ millimeters}$$

Table II gives the calculated results for $\Delta\theta$ for a number of energies. Using the results for 0.5 electron volts, which is at the other end of the observed energy spectrum, the spread in image size is:

$$5.763 \times 10^{-4} \times 64.497 \times 2.54 \times 10$$
$$+ 3.840 \times 10^{-4} \times 59.503 \times 2.54 \times 10$$
$$= .944 + .580 = 1.52 \text{ millimeters}$$

Thus the image size is slightly more than three millimeters, and the slit is more than wide enough to receive the whole image.

It is desirable to know what the energy spread is. In Chapter II it was mentioned that Bragg's law could be written as

$$\frac{h}{\sqrt{2\,m\,E}} = 2\,d\,\sin\theta$$

This expressed the relation between the energy of the neutrons and the glancing angle. Solving the expression for E:

$$E = \frac{h^2}{8\,m\,d^2\,\sin^2\theta}$$

From which $\Delta E = -\dfrac{2\,h^2\,\sin^{-3}\theta \quad \cos\theta\,\Delta\theta}{8\,m\,d^2}$

$$\Delta E = -\frac{2\,h^2}{8\,md^2} \qquad \frac{\cot\theta}{\sin^2\theta}\,\Delta\theta$$

$$\frac{\Delta E}{E} = -2 \cot \theta \Delta \theta$$

A summary of calculations based on this expression is given in Table II.

Table II is a complete summary of all the calculations made relative to the resolution of the instrument. The first column is a list of various energies for which the cross section of holmium was measured. The second column gives the corresponding glancing angle. The third column shows the change of the radius of curvature of the crystal with energy. The fourth and fifth columns give the calculated results for the spread in glancing angle in minutes and radians respectively. The sixth column gives the resolving power, $\frac{\Delta E}{E}$, and the last column gives the actual energy spread, ΔE. It can be seen that the resolving power is very good. At the most disadvantageous energy setting, 0.5 electron volts, the spread is only about three per cent, while at 0.026 electron volts it is less than one per cent. The resolving power is more than sufficient to permit neglecting the correction of the holmium data for energy spread. If a narrow, high resonance had been found, this would not necessarily be true. A comparison of the results obtained with this instrument in the case of cadmium has previously been made in Chapter II. The comparison shows that the resolution of our instrument is as good as that of other investigators.

TABLE II

THE CALCULATED RESOLVING POWER OF THE CRYSTAL SPECTROMETER ACROSS THE ENERGY SPECTRUM

Energy E	Glancing Angle θ	Radius of Crystal Curvature	Variation in Glancing Angle $\Delta\theta$		Resolving Power	Variation in Energy ΔE
Electron Volts	Degrees and Minutes	Inches	Minutes	Radians x 10^4	$\frac{\Delta E}{E}$ x 10^3	Electron Volts
			2.85	8.294	-7.749	-0.000201
0.026	12° 4'	296.2	-0.44	-1.277	1.193	0.000031
			2.77	8.056	-7.838	-0.000219
0.028	11° 37'	307.9	-0.52	-1.504	1.632	0.000046
			2.80	8.154	-8.224	-0.000247
0.030	11° 13'	318.7	-0.66	-1.929	1.945	0.000058
			2.72	7.916	-8.770	-0.000316
0.036	10° 14'	349.0	-0.64	-1.850	2.050	0.000074
			2.63	7.655	-4.7003	-0.000207
0.044	9° 15'	385.7	-0.72	-2.108	2.589	0.000114
			2.57	7.474	-9.807	-0.000490
0.050	8° 40'	411.4	-0.76	-2.219	2.902	0.000145
			2.54	7.384	-10.08	-0.000583
0.054	8° 20'	427.8	-0.80	-2.342	3.20	0.000173
			2.51	7.300	-10.32	-0.000599
0.058	8° 3'	442.7	-0.83	-2.412	3.411	0.000198

TABLE II (continued)

THE CALCULATED RESOLVING POWER OF THE CRYSTAL SPECTROMETER ACROSS THE ENERGY SPECTRUM

Energy E	Glancing Angle θ	Radius of Crystal Curvature	Variation in Glancing Angle $\Delta\theta$		Resolving Power	Variation in Energy ΔE
Electron Volts	Degrees and Minutes	Inches	Minutes	Radians x 10^4	$\frac{\Delta E}{E}$ x 10^3	Electron Volts
0.060	7° 55'	450.2	2.50 -0.84	7.265 -2.452	-10.45 3.527	-0.000627 0.000212
0.070	7° 19'	486.9	2.44 - 0.90	7.096 -2.610	-11.05 4.065	-0.000774 0.000285
0.084	6° 41'	532.7	2.38 -0.95	6.915 -2.777	-11.83 4.752	-0.000994 0.000399
0.100	6° 7'	581.9	2.32 -1.00	6.751 -2.900	-12.60 5.412	-0.001260 0.000541
0.140	5° 10'	688.5	2.22 -1.09	6.471 -3.182	-14.31 7.038	-0.002003 0.000985
0.200	4° 19'	823.7	2.18 -1.21	6.349 -3.524	-16.82 9.337	-0.003364 0.001867
0.300	3° 32'	1006	2.06 -1.25	5.998 -3.623	-19.43 11.73	-0.005829 0.003519
0.500	2° 44'	1300	1.98 -1.32	5.763 -3.840	-24.41 16.09	-0.01221 0.008045

CHAPTER IV

STATISTICAL ACCURACY

The statistical error has been computed for most of the measurements and, with two exceptions, this error is around one per cent. The two exceptions, at E = 0.3 electron volts and E = 0.5 electron volts, have a statistical error of about three and six per cent respectively. The less favorable counting conditions at these higher energies, as described under the section on "Apparatus and Procedure," are responsible for the poorer statistics.

The development of the formula used in computing statistical error follows the method developed by Rose and Shapiro.[1] Using the nomenclature of the Introduction, the expression for the cross section is:

$$\sigma = \frac{-\ln T}{nt}$$

The assumption is made here that the error in the quantity nt, which is the number of atoms per square centimeter, is negligible. Applying the law of propagation of error to this expression, we obtain:

$$\left(\frac{\Delta\sigma}{\sigma}\right)^2 = \left(\frac{\partial\sigma}{\partial T}\ \frac{\Delta T}{\sigma}\right)^2 = \left(-\frac{1}{nt\,\sigma}\ \frac{\Delta T}{T}\right)^2 = \left(\frac{\Delta T}{T \ln T}\right)^2$$

Since ln T is known from the data, it remains to obtain an

---

[1]M. E. Rose and M. M. Shapiro, "Statistical Error in Absorption Experiments," The Physical Review, 74:1853-1864, 1948.

expression for $\frac{\Delta T}{T}$.

From the Introduction, the expression for the transmission is:

$$T = \frac{I - \beta}{I_o - \beta_o}$$

Applying the law of propagation of error to this expression:

$$\left(\frac{\Delta T}{T}\right)^2 = \left(\frac{\partial T}{\partial I}\ \frac{\Delta T}{T}\right)^2 + \left(\frac{\partial T}{\partial I_o}\ \frac{\Delta I_o}{T}\right)^2 + \left(\frac{\partial T}{\partial \beta}\ \frac{\Delta \beta}{T}\right)^2 + \left(\frac{\partial T}{\partial \beta_o}\ \frac{\Delta \beta_o}{T}\right)^2$$

Steps indicated in this expression follow:

$$\frac{\partial T}{\partial I} = \frac{1}{I_o - \beta_o}, \quad \left(\frac{\partial T}{\partial I}\ \frac{\Delta I}{T}\right)^2 = \frac{\Delta I^2}{(I_o - \beta_o)^2}\ \frac{(I_o - \beta_o)^2}{(I - \beta)^2} = \frac{\Delta I^2}{(I - \beta)^2}$$

$$\frac{\partial T}{\partial I_o} = \frac{I - \beta}{(I_o - \beta_o)^2}, \quad \left(\frac{\partial T}{\partial I_o}\ \frac{\Delta I_o}{T}\right)^2 = \frac{(I - \beta)^2}{(I_o - \beta_o)^2}\ \frac{(\Delta I_o^2)\ (I_o - \beta_o)^2}{(I - \beta)^2} = \frac{(\Delta I_o)^2}{(I_o - \beta_o)^2}$$

$$\frac{\partial T}{\partial \beta} = \frac{-1}{I_o - \beta_o}, \quad \left(\frac{\partial T}{\partial \beta}\ \frac{\Delta \beta}{T}\right)^2 = \frac{(\Delta \beta)^2}{(I_o - \beta_o)^2}\ \frac{(I_o - \beta_o)^2}{(I - \beta)^2} = \frac{(\Delta \beta)^2}{(I - \beta)^2}$$

$$\frac{\partial T}{\partial \beta_o} = \frac{-(I - \beta)}{(I_o - \beta_o)^2}, \quad \left(\frac{\partial T}{\partial \beta_o}\ \frac{\Delta \beta_o}{T}\right)^2 = \frac{(I - \beta)}{(I_o - \beta_o)^2}\ \frac{(\Delta \beta_o)\ (I_o - \beta_o)}{(I - \beta)^2} = \frac{(\Delta \beta_o)^2}{(I_o - \beta_o)^2}$$

$$\left(\frac{\Delta T}{T}\right)^2 = \frac{\Delta I^2 + \Delta \beta^2}{(I - \beta)^2} + \frac{\Delta I_o^2 + \Delta \beta_o^2}{(I_o - \beta_o)^2}$$

It is now desirable to find suitable expressions for $(\Delta I)^2$, $(\Delta \beta)^2$, $(\Delta I_o)^2$, and $(\Delta \beta_o)^2$ so that one may solve for $\frac{\Delta T}{T}$.

Let the general expression for a counting rate be r_i.

Then

$$r_i = \frac{c_i}{t_i}$$

where C_i is the total number of counts and t_i is the total counting time.

$$r_i = \frac{1}{t_i} \Delta C_i$$

$$\frac{\Delta r_i}{r_i} = \frac{\Delta C_i}{t_i} \frac{t_i}{C_i} = \frac{\Delta C_i}{C_i}$$

$$\Delta r_i = \frac{\Delta C_i}{C_i} r_i = \frac{\Delta C_i}{C_i} \frac{C_i}{t_i} = \frac{\Delta C_i}{t_i}$$

$$\left(\Delta r_i\right)^2 = \left(\frac{\Delta C_i}{t_i}\right)^2$$

$$\Delta C_i = \frac{C_i}{\sqrt{C_i}} = \sqrt{C_i}, \quad \left(\Delta C_i\right)^2 = C_i$$

$$\left(\Delta r_i\right)^2 = \frac{C_i}{t_i^2}$$

$$\left(\Delta r_i\right)^2 = \frac{r_i t_i}{t_i^2} = \frac{r_i}{t_i}$$

Putting this result into the above equation for $\frac{\Delta T}{T}$ gives the working expression:

$$\frac{\Delta T}{T} = \sqrt{\frac{(I/t_I) + (\beta/t_\beta)}{(I - \beta)^2} + \frac{(I_o/t_{I_o}) + (\beta_o/t_{\beta_o})}{(I_o - \beta_o)^2}}$$

$$\frac{\Delta T}{T} = \frac{1}{I-\beta} \sqrt{\frac{I}{t_I} + \frac{\beta}{t_\beta} + T^2 \left[\frac{I_o}{t_{I_o}} + \frac{\beta_o}{t_{\beta_o}}\right]}$$

This expression for $\frac{\Delta T}{T}$ is then put into the expression developed for $\frac{\Delta \sigma}{\sigma}$ and the statistical error is computed from the resulting formula:

$$\frac{\Delta \sigma}{\sigma} = \frac{1}{\ln T} \frac{1}{I-\beta} \sqrt{\frac{I}{t_I} + \frac{\beta}{t_\beta} + T^2 \left[\frac{I_o}{t_{I_o}} + \frac{\beta}{t_{\beta_o}}\right]}$$

The statistical error was computed for all the energies at which the cross section of holmium was measured. The results are shown in Table III. With the exception of the three highest energies measured, the statistical error is held to about one per cent. The increasing error at 0.2, 0.3, and 0.5 electron volts emphasizes what was said in Chapter II about the poorer statistical conditions at these higher energies.

Errors arise from causes other than statistics. For example there is a fluctuation in pile power and instrumental deficiencies such as the sample shifter so that the statistical error should be multiplied by a factor of at least two in order to obtain an estimated total error.

CHAPTER V

PURITY OF SAMPLE

The material was in the oxide form, Ho_2O_3. A water analysis revealed that the raw material contained roughly six per cent water. It was decided that the experiment would not be feasible with so much water present because of the high scattering cross section of water. It was decided, therefore to prepare anhydrous samples.

The samples were heated at 900°C and transferred to a drybox for loading into the glass capillary tubes. The tubes were kept in sealed off containers prior to use. After being mounted in the wafer, the friction fit of the aluminum plugs, aided by silicone lubricant and gaskets were depended upon for keeping the sample dry. Justification in this dependence came when the first energy measured was repeated after a period of two weeks. There was no change in the transmission within the statistical accuracy, thus showing that no water was being picked up by the sample.

The samples were furnished by Dr. Boyd and Mr. Darwin Harris of Oak Ridge National Laboratory Chemistry Division. They were separated by the ion exchange column technique and are extremely pure. Impurities are believed present in less than one part per million.

CHAPTER VI

RESULTS

The results of the experiment are given in Table III. Included in this table is the computed statistical error. The cross section results are plotted versus neutron energy in Figure 25. Since the material was in the oxide form, it was necessary to subtract off the effect due to oxygen in order to get the cross section for holmium alone. In making this correction, the cross section of elemental oxygen as a function of energy was used. This is not strictly accurate but is true to a good approximation since the effect due to oxygen is small, the cross section of oxygen being about four barns.[1]

A plot of the preliminary data in the energy region near 0.06 electron volts showed a small rise in the curve which was outside the statistical error. A crystalline diffraction peak was then looked for in this region, and found. Further investigation revealed a group of these peaks near 0.03 electron volts. Figure 24 shows the data plotted in this manner. The crystalline diffraction peaks are evident in both Figure 24 and Figure 25. Since the effect of these peaks is only about three per cent of the total cross section the accumulation of sufficient data to determine accurately their energy positions and height would have required very long periods of time.

---

[1]H. H. Goldsmith, H. W. Ibser, and B. T. Feld, op. cit., p. 267.

TABLE III

RESULTS OF TRANSMISSION MEASUREMENTS ON HOLMIUM

Energy E in Electron Volts	Transmission $T\left(\frac{E}{W}\right)$	$-\ln T\left(\frac{E}{W}\right)$	$\frac{\Delta\sigma}{\sigma}$	Cross Section σ for Holmium in Barns per Atom	Sample Number
.026	.3055	1.1858	.0131	92.66	1
.028	.3169	1.1492	.0119	89.61	1
.029	.3233	1.1292	.00949	87.94	1
.0292	.3241	1.1267	.00775	87.73	1
.0294	.3288	1.1123	.0104	86.53	1
.0296	.3228	1.1307	.0122	88.07	1
.0298	.3278	1.1154	.00833	86.79	1
.030	.3190	1.1426	.0102	89.06	1
.03025	.3324	1.1014	.0110	85.69	1
.0304	.3162	1.1514	.00628	89.80	1
.031	.3311	1.1056	.0103	85.98	1
.035	.3472	1.0579	.0103	82.07	1
.036	.3488	1.0533	.00991	81.68	1
.040	.3723	.9881	.0102	76.31	1
.044	.3801	.9673	.0074	74.73	1
.050	.4039	.9066	.00756	69.66	1
.054	.4184	.8713	.00625	66.79	1
.055	.4084	.8955	.00596	66.81	1
.056	.4123	.8860	.00784	68.02	1
.058	.4194	.8689	.00852	66.67	1
.070	.4586	.7796	.00821	59.21	1
.084	.4899	.7136	.00933	53.78	1
.10	.5116	.6702	.00931	50.16	1
.14	.5572	.5848	.0128	43.11	1
.20	.6002	.5105	.0192	36.91	1
.30	.6555	.4224	.0333	29.55	1
.50	.6665	.4057	.0619	28.20	1
.0715	.6018	.5078	.0091	60.81	2
.14	.6949	.3640	.0111	42.1	2
.114	.6630	.4110	.0130	48.21	2

UNCLASSIFIED
Dwg. 8901

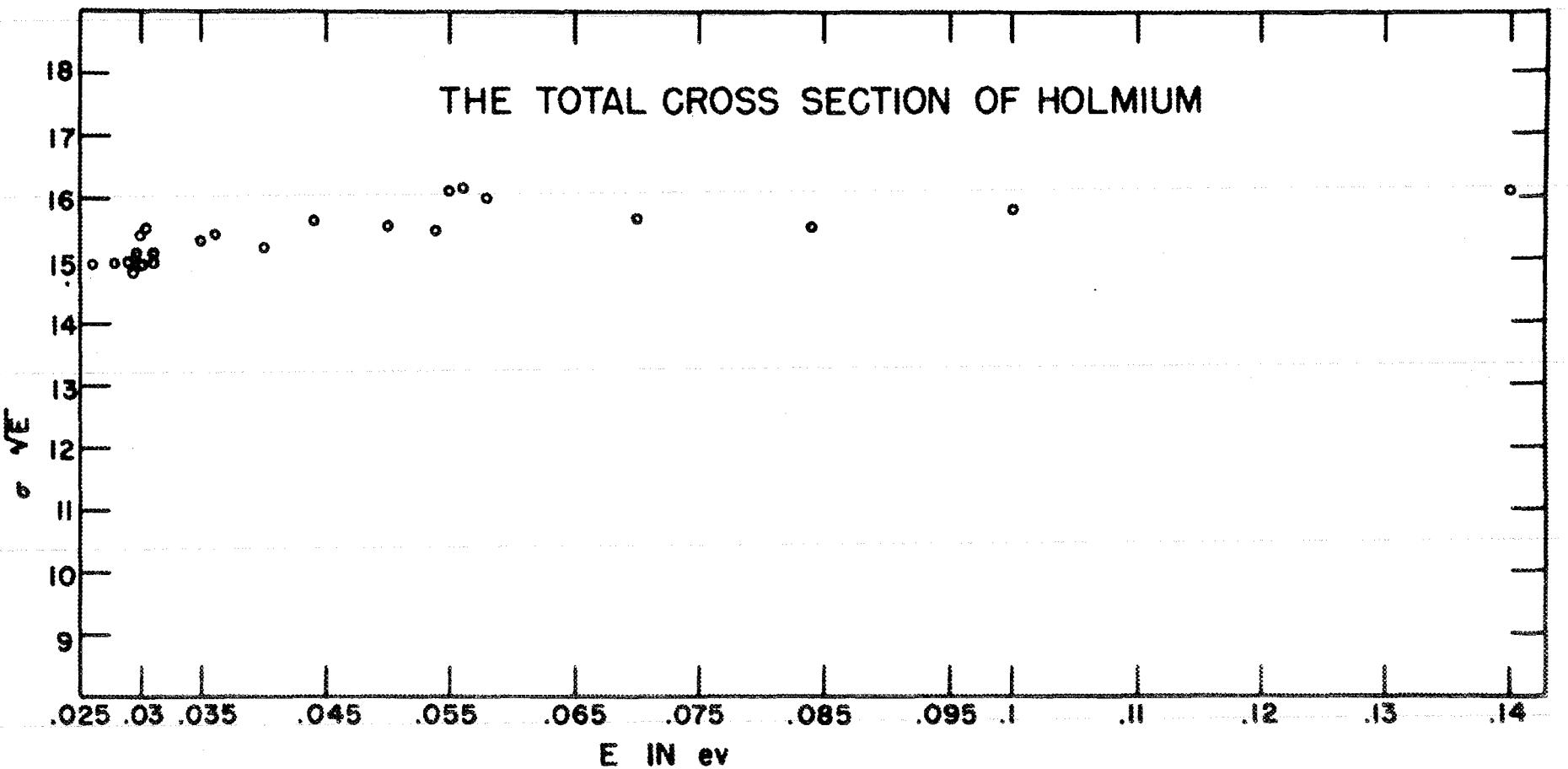

FIGURE 24

FIGURE 25

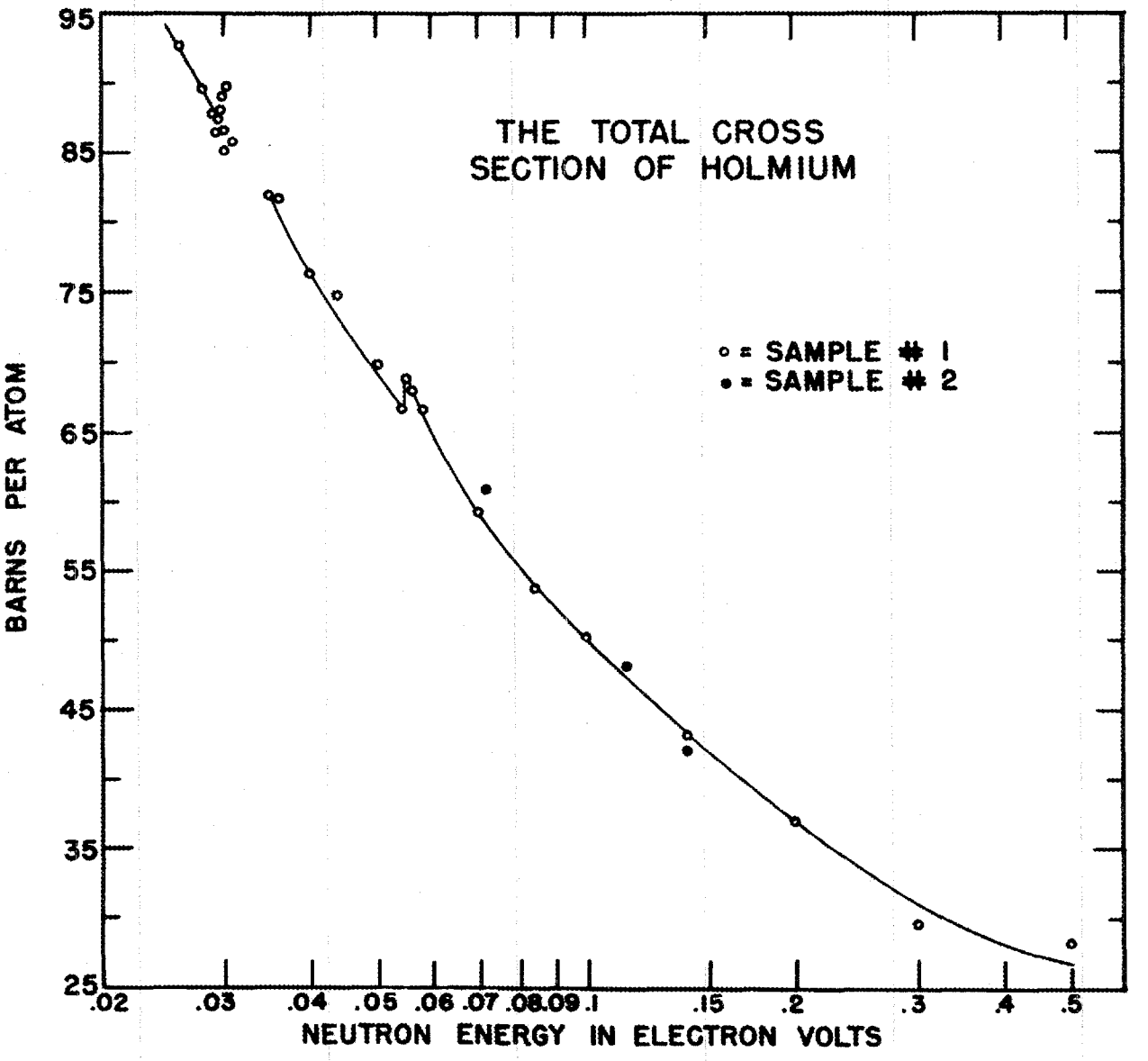
THE TOTAL CROSS SECTION OF HOLMIUM
○ = SAMPLE # 1
● = SAMPLE # 2
BARNS PER ATOM
95
85
75
65
55
45
35
25
.02
.03
.04
.05
.06
.07
.08
.09
.1
.15
.2
.3
.4
.5
NEUTRON ENERGY IN ELECTRON VOLTS

However, the existence of such peaks due to the crystal structure in this energy region is consistent with the interpretation given below that holmium has a high scattering cross section.

As indicated in Table III and Figure 25, most of the data was taken with the first sample, which is called sample number one. Sample number one weighed 0.0668 grams which gives an nt value of 11.98×10^{21} holmium atoms per square centimeter. Transmission measurements were taken on a second sample for the purpose of checking results achieved with the first. The second sample weighed 0.042 grams which gives an nt of 7.618×10^{21} atoms per square centimeter. Three energies were studied with the second sample, one of which had been measured previously with sample number one. The answers obtained with the two samples are within the statistical accuracy. The other two points measured with sample number two fall on the curve of the first sample. The answer most at variance is the one at 0.0715 electron volts. Even here the discrepancy is only about two and one half barns and there is a possibility of a crystalline diffraction peak at this point.

The plan originally was to measure the neutron cross section of holmium as a function of energy between 0.03 electron volts and 0.3 electrons volts, the reason for these limits having been discussed previously in the chapter on Apparatus and Procedure. It was decided

to extend these limits, after considerable data had been taken, because of the unusual character of the results.

It was mentioned in the Introduction that Mr. H. Pomerance had measured the absorption cross section for thermal neutrons (average energy 0.025 electron volts) at sixty-four barns. It was somewhat disturbing, then, to find a total cross section of 89 barns at 0.03 electron volts. The extrapolated answer at 0.025 electron volts would have been about 95 barns. This would have meant a nuclear scattering cross section of about 31 barns, much higher than one has any right to expect. Dr. C. Shull of the Physics Division of Oak Ridge National Laboratory then suggested, on the basis of work recently done at Columbia, that this answer was perfectly reasonable because of paramagnetic scattering.[2, 3]

There are two types of paramagnetic substances. There is a large group of substances which includes many of the metallic elements whose paramagnetism is dependent upon whether they are in the solid conducting states. In these substances the electrons in the outer shell are loosely bound and become conduction electrons in a solid metal or valence electrons in a chemical compound. In a metal the spins of a portion of these outer orbital electrons can be aligned by

---

[2] I. W. Ruderman, W. W. Havens, Jr., T. I. Taylor, and L. J. Rainwater, "The Scattering of Slow Neutrons by Paramagnetic Crystals," The Physical Review, 75:895, 1949.

[3] I. W. Ruderman, "The Scattering of Slow Neutrons by Paramagnetic Crystals," The Physical Review, 76:1572-1584, 1949.

an applied magnetic field. A good example of this group is sodium. Such substances are said to be weakly paramagnetic.

Usually the inner electron shells are full so that the magnetic moments due to their orbital and spin angular momenta are such as to cancel out so that ordinarily these inner electron shells contribute only to atomic diamagnetism. This is not always the case however. For example, the iron group, the palladium and platinum group, and the rare earths have inner shells which are incomplete and therefore have a resultant moment which is large compared with the spin of the valence electrons or the diamagnetism of a closed shell. Such substances are said to be strongly paramagnetic. The most strongly paramagnetic substances are the trivalent ions of dysprosium and holmium which have magnetic moments of more than ten Bohr magnetons.[4] These elements belong to the rare earths, which from cerium 58 to ytterbium 70 have an unfilled 4f subshell of the fourth electron shell in the trivalent state. The electrons in this unfilled inner shell are well protected from the influence of atomic neighbors by the outer electron shells.

The neutron has a magnetic moment and may be thought of as a magnetic dipole. Holmium has a very large magnetic moment and produces a powerful dipole. The interaction of these dipoles results in a scattering of the incident neutrons. This is an atomic phenomenon, a scattering of neutrons by orbital electrons as distinguished from a

---

[4]R. M. Bozorth, "Magnetism," Reviews of Modern Physics, 19:68, 1947.

nuclear process. It occurs in paramagnetic substances and is called paramagnetic scattering or simply magnetic scattering.

It is possible to get a rough idea of the magnitude of the paramagnetic scattering for holmium. Assume that the total cross section is made up of three components:

$$\sigma_{\text{total}} = \frac{C}{\sqrt{E}} + \sigma_s + \sigma_{pm}$$

where $\frac{C}{\sqrt{E}}$ is the absorption cross section, σ_s is the constant nuclear scattering cross section, and σ_{pm} is the paramagnetic scattering cross section. Actually, the paramagnetic scattering cross section is not constant, but decreases with increasing energy. At 0.025 electron volts the absorption cross section, σ_a, is 64 barns.[5] From this we can evaluate C:

$$\frac{C}{\sqrt{0.025}} = 64$$

$$C = 10.11 \text{ barns} - (\text{electron volts})^{\frac{1}{2}}$$

Since the paramagnetic scattering should be negligible at 0.5 electron volts, it was decided to measure the total cross section there. Setting σ_{pm} equal to zero we have:

$$\sigma_{\text{total}} = 28.2 = \frac{C}{\sqrt{E}} + \sigma_s = \frac{10.11}{\sqrt{0.5}} + \sigma_s$$

$$\sigma_s = 13.9 \text{ barns, nuclear scattering}$$

---

[5]H. Pomerance, loc. cit.

The measured total cross section at 0.03 electron volts was 89 barns. We can now write the following:

$$\sigma_{total} = 89 = \frac{C}{\sqrt{E}} + \sigma_s + \sigma_{pm} = \frac{10.11}{\sqrt{0.03}} + 13.9 + \sigma_{pm}$$

From this expression, σ_{pm} is about 17 barns at 0.03 electron volts.

A measurement was taken at 0.026 electron volts, in spite of the higher order effect, and here the effect is still about 16 barns. In the absence of the higher order effect it is believed the observed result would have been about 19 barns. Figure 24, a plot of $\sigma\sqrt{E}$, may be compared with Figure 14. The lack of dropping off of the curve below 0.03 in the case of Ho indicates that paramagnetic scattering, which increases with decreasing energy, is holding up the curve.

In a recent communication, Dr. E. P. Wigner suggests that perhaps the cross section measurements on holmium could be accounted for by the presence of a scattering resonance at negative energy. Unfortunately, the type of data furnished by the technique used in taking these measurements is not suited to making a unique choice between the two proposed explanations, paramagnetic scattering or a scattering resonance at negative energies. Nuclear scattering of slow neutrons is isotropic and very sharply dependent upon energy in the vicinity of a resonance. The paramagnetic scattering, however, depends upon the atomic form factor of the electrons producing the paramagnetism, and therefore its intensity falls off as the scattering angle increases. A study of the scattering cross section of holmium as a function of scattering angle and energy could perhaps choose between the two proposed explanations. A use of the technique of this experiment in order to make the choice would involve studying the detailed structure of the cross section, preferably at longer wave lengths.

BIBLIOGRAPHY

BIBLIOGRAPHY

Bernstein, S., Dial, J. B., Stanford, C. P., and Stephenson, T. E. "Total Cross Sections of Small Samples of Hf, Er, Ni^{58}, and Ni^{60} from Neutron Crystal Spectrometer Measurements," The Physical Review, 75:1302, 1949.

Borst, L. B., Ulrich, A. J., Osborne, C. L., and Hasbrouck, B. The Physical Review, 70:108, 1946.

Bothe, W. Z. Naturforch 1, 179, 1946.

Bozorth, R. M. "Magnetism," Reviews of Modern Physics, 19:29-86, 1947.

Buerger, Martin. X-Ray Crystallography. New York: John Wiley and Sons, Ins., 1942.

Compton, Arthur H., and Allison, Samuel K. X-Rays in Theory and Experiment. New York: D. Van Nostrand Company, Inc., 1946.

Goldsmith, H. H., Ibser, H. W., and Feld, B. T. "Neutron Cross Sections of the Elements." Reviews of Modern Physics, 19:259-297, 1947.

Hoover, J. I., Jordan, W. H., Moak, C. D., Pardue, L., Pomerance, H., Strong, J. D., and Wollan, E. O., "Measurement of Neutron Absorption Cross Sections, with a Pile Oscillator," The Physical Review, 74:886-870, 1948.

Jenkins, Francis A., and White, Harvey E. Fundamentals of Physical Optics. New York: McGraw Hill Book Company, Inc., 1937.

Rose, M. E., and Shapiro, M. M. "Statistical Error in Absorption Experiments," The Physical Review, 74:1853-1864, 1948.

Ruderman, I. W., Havens, W. W., Jr., Taylor, T. I., and Rainwater, L. J. "The Scattering of Slow Neutrons by Paramagnetic Crystals," The Physical Review, 75:895, 1949.

Ruderman, I. W. "The Scattering of Slow Neutrons by Paramagnetic Crystals," The Physical Review, 76:1572-1584, 1949.

Seren, Leo, Friedlander, Herbert N., and Turkel, Solomon H. "Thermal Neutron Activation Cross Section," The Physical Review, 72:888-901, 1947.

Wyckoff, Ralph W. Structure of Crystals. New York: Reinhold Publishing Corporation, 1935.